Review of rainwater infiltration rates in wall assemblies

Stéphanie Van Linden*, Nathan Van Den Bossche

Ghent University, Faculty of Engineering and Architecture, Building Physics Research Group, Belgium

Abstract

Detailed knowledge on expected infiltration percentages through various exterior cladding surfaces is of importance when conducting hygrothermal simulations to evaluate the long-term performance of wall assemblies. Due to the stochastic nature of rainwater infiltration through wall assemblies, it is not possible to precisely predict the amount of rainwater that will infiltrate. However, laboratory and field tests may provide insight into the range of infiltration rates that can be expected for a given cladding and insight into the impact of deficiencies and the parameters affecting infiltration. Therefore, quantitative studies concerning infiltration rates, which were mostly laboratory studies, were reviewed. Based on the reviewed studies, the driving forces for infiltration were determined and the impact of the applied test method, pressure difference and water deposition rate on the infiltration rates was analysed. A methodology to obtain information on infiltration percentages without performing additional laboratory tests was proposed and a categorization of cladding materials was developed.

Keywords: Rainwater infiltration, hygrothermal simulation, watertightness test method, water entry function

1. Introduction

Rainwater infiltration through wall assemblies and through deficiencies in the watertightness of the building envelope are the most common causes of premature building deterioration. Rainwater may infiltrate across the exterior cladding surface through intentional or unintentional openings. When the infiltrated rainwater is not managed properly or an excessive amount of water infiltrates due to execution defects, damage to underlying elements may be caused [1]–[4]. To assess the risk of damage caused by infiltrating rainwater and to evaluate the long-term performance of wall assemblies, hygrothermal simulations may be carried out. These simulations can be conducted by 1D, 2D or 3D hygrothermal simulation software, for example WUFI [5], [6] or DELPHIN [7]. To perform hygrothemal simulations, detailed knowledge on the response of wall assemblies to impinging and infiltrating rainwater is necessary [8], [9].

During a rain event, raindrops may impinge the exterior surface of a wall assembly due to the co-occurrence of wind and rain. The amount of water hitting the exterior cladding surface depends on the façade geometry, the wind

*Corresponding author
Email address: stephanie.vanlinden@ugent.be
Postal address: Sint Pietersnieuwstraat 41, B4, 9000 Gent, Belgium

velocity and the rain intensity and has already been studied extensively [10]–[20]. When raindrops hit the exterior surface of a wall assembly parts of the drops may spread out over the exterior surface (1a), splash open and separate into different smaller drops (1b) or rebound of the exterior surface (1c) immediately after impacting the surface, they may be absorbed by the exterior surface (2a) and evaporate (2b), runoff along the exterior surface due to gravity (3a) or adhere to the surface (3b), or infiltrate through the cladding (4) (Figure 1).

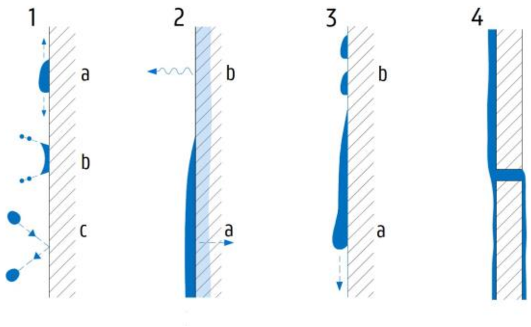

Figure 1: Occurring phenomena after raindrops impact the exterior cladding surface of a wall assembly

The different phenomena which may occur after raindrops have impacted the exterior cladding surface of a wall assembly are shown in Figure 1 as four scenarios. Each of these scenarios has already been studied in literature:

1. Abuku et al. [21], Couper [22] and many others, for example [23]–[27], have researched splashing, spreading and bouncing of impinging raindrops. Abuku et al. [21] performed experiments to investigate how a drop behaves immediately after impacting on a porous surface. It was concluded that a drop with a diameter of 3,9 mm splashed when impinging the porous surface and that a drop with a small impact angle and speed bounced off the surface. Couper [22] reported results of field tests for various panel surfaces and found that higher rain intensities resulted in higher splash percentages. Similarly, Mason and Andrews [28] found that the presence of a thin water film on the surface increased the splash percentage and Mutchler and Hansen [29] reported that the splash size increased for increasing water film depth.
2. Porous cladding materials, for example bricks, may absorb, store and release rainwater by evaporation. Water may be absorbed at the exterior cladding surface due to capillary action and be transported further into the material through its pores. When all the open pores are filled with water, the material is saturated. The time before saturation occurs depends on the sorptivity of the material and the rain intensity [30]–[38].
3. Water runoff occurs on non-absorptive surfaces, for example glass, and fully-saturated exterior surfaces, for example saturated masonry brick wall. When several impinging drops adhere to the surface, spread out and

coalesce, a film may be formed which will flow down when the gravitational forces exceed the surface tension forces. Blocken et al. [39] provide an extensive review on the available literature concerning rainwater runoff.

4. Water may also infiltrate through the cladding, either through intentional or unintentional openings present in a non-absorptive cladding or fully saturated cladding material. Intentional openings can for example be open joints between panel cladding. Unintentional openings can be present as for example cracks in the cladding surface or deficiencies at the interface between different building components. Wind-driven raindrops may flow directly through large intentional openings ($\geq$ 8 mm) [40] or water may infiltrate through smaller unintentional openings (< 8 mm) due to an external driving force, for example a hydrostatic pressure caused by water runoff over the opening or wind pressure. Van Den Bossche et al. [41] and Calle and Van Den Bossche [42] have calculated the expected driving forces necessary for water to infiltrate through round openings and cracks represented by slits in a polycarbonate and PMMA panel. Olsson and Hagenthoft [43] have developed an algorithm to calculate the expected infiltration rates through an opening with a given geometry and validated the model by means of experimental data measured for openings in fibre cement panels and polycarbonate panels with and without a dam [44].

When water that has infiltrated through the cladding is not managed properly, it may reach parts of the wall assembly where it can cause damage or decreased performance, for example to structural parts of the assembly or to insulation materials. To reduce the risk of damage, either sufficient drainage capacity should be provided and/or materials should be used able to resist wetting by the infiltrated water. To predict the drainage capacity and the resistance to wetting, drainage tests and hygrothermal simulations respectively, may be conducted. However, to be able to do these drainage tests and to perform hygrothermal simulations, detailed knowledge of the expected infiltration rates is required for various types of cladding [45]–[50].

Many field and laboratory studies have already been conducted with regard to water management and water infiltration through various cladding types, for example [51]–[64], and façade components and their interfaces, for example [65]–[77]. However, most studies are qualitative in nature, only focus on one or at most two types of cladding or do not provide quantitative information on the infiltration rates or infiltration percentages.

Due to the lack of quantitative data for various types of cladding materials, ASHRAE Standard 160 “Criteria for Moisture-Control Design Analysis in Buildings” [78] proposes a default penetration rate of 1% of the rain impinging onto the cladding to be used as a moisture load in hygrothermal simulations. The proposed deposit site for the moisture load is the exterior surface of the weather-resistive barrier (WRB). It is assumed that the infiltration rate implicitly accounts for any drainage in front of the WRB, for example water running down on the back side of the exterior cladding, but no drainage on the WRB itself is accounted for. If a weather-resistive barrier is not provided, then the deposit site shall be based on a technical rationale. No differentiation is made for different exterior surfaces. Additionally, the 1% penetration rate was proposed for a North American context in which construction types differ from those in other continents around the world, for example in contrast with North-America, ventilated facades with open joints are widely used in Europe which typically allow a larger percentage of water to infiltrate across the exterior cladding surface and potentially reach the weather-resistive barrier than for example EIFS (Exterior Insulation and Finish System). Hygrothermal simulations accounting for water infiltration may be conducted taking into account a rainwater penetration load as a percentage of the wind-driven load on the exterior surface or taking into account a retention percentage based on the portion of water that is retained to the WRB after drainage of infiltrated water [45], [79]. However, due to the lack of information on infiltration rates for various exterior cladding surfaces, 1% of the wind-driven rain load is typically chosen as rainwater penetration load and deposited on the weather-resistive barrier to evaluate the impact of rainwater infiltration on the long-term performance of wall assemblies [8], [9], [48], [49], [80], [81]. This emphasizes the need for a method to estimate the expected infiltration rates through various cladding types and the deposit site in more detail.

This paper provides a review of quantitative research on infiltration rates through various types of cladding and through joints at façade details. The review is preceded by an overview of watertightness test procedures and a section on the correlation between test parameters and climate conditions. Based on the review of laboratory and field studies, the driving forces for infiltration are determined and the impact of the applied test method, pressure difference and water deposition rate on the infiltration rates is analysed. A categorization of cladding materials is then developed to obtain information on infiltration percentages without performing additional laboratory tests.

2. Watertightness test procedures

Experimental studies that have quantified infiltration percentages are either laboratory studies or field studies. Sahal and Lacasse [82], Recatala et al. [83] and Van Den Bossche [84] provide an overview of existing laboratory test procedures to evaluate the watertightness performance of wall assemblies. These procedures either describe static, cyclic, dynamic or wind tunnel tests. In all procedures wind is simulated by the application of an air pressure difference over the test sample and rain is provided by spraying water either directly onto the specimen (first three procedures) or by releasing waterdrops in an air stream flowing over the test specimen during wind tunnel testing. Static and cyclic test procedures are most commonly applied to evaluate the watertightness of wall assemblies.

During a static test (for example EN 1027 [85]), a pressure difference is maintained over the test specimen for a specified period of time (5-15 minutes) and stepwise increased up to the required performance level (typically between 0-1200 Pa). A spraying system provides a water load onto the specimen with a constant spray rate. In Europe a uniform spray rate of 2.0 L/min.m^2 is commonly applied whereas in North-America a spray rate of 3.4 L/min.m^2 is prescribed. Whereas static tests prescribe a stepwise increasing but constant pressure difference, the cyclic tests (for example EN 12865 [86]) prescribe rapid pressure pulses between a lower and upper limit. During both the static and cyclic test procedure, the test samples should be visually observed and the time, infiltration location and air pressure difference when water infiltrates should be reported. EN 12865 also states that if required the water absorbed by the test specimen during the test shall be determined by weighing the specimen before and after exposure to driving rain. It should be noted that these test standards and procedures have been developed with the aim to assess the performance threshold with a pass/fail criterion. Hence, the ‘watertightness’ is conceived as an absolute concept: a construction is watertight up to a certain pressure difference regardless of the indoor climate, susceptibility of materials to premature degradation, moisture storage, or other variables. Hence, the quantification on infiltration rates is not explicitly within the scope of the standards, and by consequence no guidelines are provided to quantify the rain water infiltration during a watertightness test procedure.

Different water delivery systems may be applied to subject the test specimens to a water load, for example multiple hydraulic nozzles that require high water pressure to form a uniform pattern on the specimen, use of air atomizing nozzles that result in a fine mist deposit, use of nozzles that deposit all the water at the top of the wall and have it cascade down the wall or use of vertical falling water combined with actual wind (provided by for example a wind tunnel). All these systems could average to the same deposition rate that is required by the test standards, but could result in different impingement scenarios and thus differences in infiltration rates. Hydraulic nozzles creating a uniform pattern on the specimens are however, most commonly applied.

Both Chew [87] and Recatala et al. [83] provide an overview of field test procedures. Similar to the samples during laboratory studies, on-site test samples should be exposed to air pressure differences and water spraying for a defined duration during field tests. Although these procedures may provide insight into the impact of on-site workmanship on the infiltration of rainwater, the performance of the test samples during the field test may still differ from the actual performance of wall assemblies exposed to realistic climate conditions in different locations

[14], [88], [89]. Therefore another group of field studies, although limited in number, have exposed test samples to actual rain events for a longer period of time and quantified the infiltration percentages [90].

3. Test parameters versus climate conditions

Although the previously mentioned test procedures are developed to impose certain climate conditions, the combination of prescribed test parameters, i.e. pressure difference, spray rate and duration, aims to represent the conditions for a specific location and return period. This implies that test parameters may be too severe for certain locations, resulting in over-dimensioned systems, or not severe enough, entailing increased risks for premature deterioration and failure. Therefore, over the past decades several researchers have developed methods to establish test parameters based on actual rain and wind loads on buildings facades.

Cornick and Lacasse [91] developed a method to calculate watertightness testing parameters based on the methodology developed by Straube and Burnett [19] and Choi [17]. Based on hourly climate data, wind-driven rain intensity (WDR) was calculated in the following manner:

$$WDR=RAF*DRF(i_h)*v(z)*i_h*\cos\vartheta \qquad (1)$$

Where: *RAF* is the Rain Admittance Factor and set to 0.9 in the study of Cornick and Lacasse, *DRF* is the Driving Rain Factor and is inversely proportional to the terminal velocity of raindrops (s/m), *v(z)* is the hourly average wind speed (m/s) for a specific height z (m), i_h is the hourly horizontal rainfall intensity (mm/h.m^2) and θ is the angle between the wind direction and the normal to the wall (°).

The driving rain wind pressure (*DRWP*) was calculated as follows:

$$DRWP=\frac{1}{2}\rho_{air}v(z)^2 \qquad (2)$$

Where: ρ_{air} is the density of air, assumed to 1.2 kg/m^3 and *v(z)* is the wind speed during rain (m/s) for a specific height z (m).

Based on calculated WDR and DRWP values for 23 Canadian locations and for return periods between 1 in 2 years and 1 in 30 years, Cornick and Lacasse [91] suggested a test protocol with pressure steps ranging from 0 to 1000 Pa, where 1000 Pa would cover most of the extreme locations for a return period of 1 in 30 years. The suggested spray rates range from 0.4 L/min.m^2 to 3.4 L/min.m^2 which cover normal in-service conditions for hourly and 5 minute events respectively. The methodology for calculating test parameters was further developed by Sahal and Lacasse [82] and Cornick et al. [12] and applied to five cities in the United states. Similar conclusions were drawn as in the study on Canadian cities. Although these studies provide insight in maximum occurring wind driven rain intensities and driving rain wind pressures, they do not provide information on the co-occurrence of rain and wind.

In general, during rain events with high rain intensities lower extreme wind speeds occur as compared to all hours in which rain is recorded. Both Pérez-Bella et al. [88], [92] and Van Den Bossche et al. [89], [93] developed a methodology to determine watertightness test parameters taking into account the co-occurrence of rain and wind based on a Bayesian performance-based analysis and a Pareto-front analysis, respectively. For more detailed information on the methodologies, please refer to [88], [93]. Van Den Bossche et al. [93] applied the Pareto-front method to two climate datasets with 10-minute values for Belgium (RMI) and the Netherlands (RNMI) at a reference height of 10 m and base wind speed of 27 m/s. The data were fitted to a statistical model, which allows to calculate extreme conditions for other durations and return periods. The obtained values for peak WDR, peak DRWP and combined average WDR and DRWP for return periods of 1 in 5 years up to 1 in 50 years are presented in Table 1.

Table 1: Test parameters for multiple return periods based on the Pareto-front analysis [93]

T (years)		**5**	**10**	**15**	**20**	**25**	**30**	**40**	**50**
RMI									
Peak WDR	WDR (mm/h)	56	69	76	80	84	87	91	94
	DRWP (Pa)	32	41	45	48	51	52	55	57
Peak DRWP	WDR (mm/h)	26	32	35	37	39	40	42	43
	DRWP (Pa)	223	276	304	324	338	350	367	380
WDR – DRWP	WDR (mm/h)	41	50	55	59	61	63	66	69
	DRWP (Pa)	128	158	175	186	194	201	211	219
RNMI									
Peak WDR	WDR (mm/h)	74	92	102	108	112	116	121	125
	DRWP (Pa)	63	81	91	97	102	106	111	115
Peak DRWP	WDR (mm/h)	10	10	10	10	10	10	10	10
	DRWP (Pa)	268	344	383	409	428	443	466	482
WDR – DRWP	WDR (mm/h)	42	51	56	59	61	63	66	68
	DRWP (Pa)	165	212	237	253	265	275	289	299

Based on the obtained values, it can be stated that a requirement of no water infiltration up to a pressure difference of 600 Pa combined with a spray rate of 2 L/min.m^2 (120 mm/h) according to EN 1027, is severe and may only occur at relatively large reference heights. A watertightness of 600 Pa is for example required by NBN B 25-002-

1:2019 for windows in Belgium when applied at the coast at a reference height of 42 m or up to 100 m in rural areas.

It is therefore, of importance to keep in mind that simultaneously subjecting test specimens to both high spray rates and high pressure differences, as prescribed by most standards, are extreme test conditions. On the other hand, high spray rates may result in a higher percentage of splashing of water onto the water film present at the specimen surface [28], [29] which could potentially reduce the amount of water available on the surface to infiltrate. The combination of low spray rates with high pressures may then result in higher infiltration percentages compared to high spray rates. However, further research is necessary to verify this hypothesis.

It would thus be more relevant to subject specimens to low spray rates (0.75 L/min.m^2) combined with high pressure differences (up to 500 Pa for a Belgian and Dutch context) and vice versa (2 L/min.m^2 and 150 Pa) as well as averaging spray rates and pressure differences depending on the fail mechanisms of the test specimens to reduce the uncertainty between laboratory testing results and performance in practice. However, at the time of writing no standards exist prescribing such test procedure.

4. Infiltration rates through the exterior cladding surface of wall assemblies

Although most often water infiltration occurs at interfaces between different building components [94], infiltration through the cladding of wall assemblies itself is not uncommon. This section provides insight into the infiltration rates through various types of cladding, i.e. sidings, ETICS, stucco, masonry, cladding panels with open joints and curtain walls. The reported infiltration rates and percentages are defined in this study as the amount of water that penetrated the exterior cladding surface and infiltrated towards the interior side of the cladding either reaching the drainage cavity and/or the drainage barrier depending on the cavity size, or in case no drainage cavity was present reaching materials that are not intended to get wet.

For each type of cladding, background information is provided and insight into the management of impinging raindrops and the different manners in which infiltration occurs is given. Based on the reported infiltration rates in literature, the impact of the pressure difference and spray rate is discussed. When available also the impact of static versus cyclic test methods on the infiltration rates is evaluated.

The reported infiltration rates are summarized in tables for each cladding type (see Appendix). These tables include information on the cladding materials, specimen size, the presence of defects, the spray rate and the pressure difference steps. The infiltration rates are given for the lowest tested pressure difference, which is in most cases 0

Pa, a medium pressure and the highest tested pressure difference ≤ 600 Pa. The infiltration percentages are then calculated as the ratio of the infiltration rate to the spray rate multiplied with the specimen area.

4.1 Sidings

Sidings, vinyl sidings or painted wood based sidings, are in itself water resistant materials. When installed in an overlapping manner, the sidings are supposed to keep out all impinging rainwater. However, water might still be able to penetrate through cracks in the siding or at poorly installed joints between two pieces of siding [95], [96]. Tsongas et al. [97] conducted a field study on a 400-unit apartment complex in the northern California Bay area, which was clad with shiplap hardboard siding. In some locations, water staining at the backside of the siding was visible. In contrast, water spray wicking tests in the laboratory showed that staining did not occur at the back of the siding. Boardman and Glass [98] also measured no water infiltration behind well-installed siding with a cavity of 11 mm, regardless of the wind speed and rain intensity. Afterwards, three defects were introduced by sliding up a wedge between the lap siding, creating a small irregular shaped gap. Absorbent pads were placed on the outside of the sheathing to detect if any water got past the siding by measuring weight gain after a rain event. At a pressure difference of 17.1 Pa no water infiltration was measured. However, at a pressure difference of 30.4 Pa water infiltration, i.e. 0.046% of the sprayed water, occurred which indicates that a pressure threshold needs to be exceeded before water is forced through the defects. Larger infiltration rates were measured for increasing pressure differences over the wall. Ngudjiharto [90] performed a field study on a direct-fixed vinyl Dutch-lap siding wall including a window with a South East orientation. The exterior of the wall was exposed to naturally occurring weather events which were monitored by a weather station. The wind-driven rain intensity was measured by means of rain gauges attached to the facade at various locations. The largest monthly total of measured wind-driven rain was close to 30 mm. The infiltrated water across the siding was collected by a trough at the bottom of the wall. Both the weather conditions and infiltration of water were measured for 7 months. The maximum percentage of infiltrated water collected by the bottom trough averaged over a one-month period was 0.27% of the wind-driven rain load. Rainwater was captured by the head J-trim of the window and was directed towards the interior underneath the window along the jamb J-trims. This emphasizes the importance of providing flashing above the window.

4.2 Exterior Thermal Insulation Composite Systems (ETICS)

External Thermal Insulation Composite Systems (ETICS) in Europe or Exterior Insulation and Finish Systems (EIFS) in North America consist of an insulation panel attached to the substrate wall, a reinforced base coat and a finish coat. During a rain event, water that impinges onto the exterior surface will almost immediately start to runoff due to the low capillary water absorption coefficient of the finish coat (< 0.1 kg/m^2 after one hour [99]). Water penetration through the face of newly installed EIFS is very unlikely [100], [101]. It is however, almost impossible to avoid cracking of the coats due to hygric stresses, embrittlement due to ageing or building movement [102]–[105] through which water can infiltrate.

When EIFS are applied to solid masonry, the masonry may absorb the infiltrated rainwater and release it by diffusion and evaporation at the interior or exterior surface. Wood frame constructions on the other hand are much more sensitive to wetting and infiltrated water may cause severe problems such as rotting of the sheathing board which acts as substrate for the EIFS in wood frame constructions. This has led to numerous damage cases [52], [106]–[108]. It is therefore, for example in North America, no longer allowed to apply EIFS on wood-frame wall assemblies without the presence of a drainage cavity. However, due to the advantages of EIFS – they are easy to install, relatively cheap and large insulation thicknesses can be obtained – the system is still widespread and has been extensively studied and improved [109]–[114].

A lot of research addresses the durability of EIFS assemblies and the water penetration resistance of interfaces at façade details, whereas limited attention has been paid to water infiltration through cracks in the render. Ullet and Brown [115] performed a static water penetration test on an EIFS specimen both with and without a horizontal defect, simulating a crack. The water infiltrating across the specimen, reaching the interior side of the EPS and draining along the drainage channels (25 x 6 mm) in the EPS and/or draining through vent openings at the bottom of the specimen (dynamic tests), was collected. Without any pressure difference, the amount of infiltrating water was the same for the specimen with and without defect (0.06%). The amount of infiltrating water increased for increasing pressure difference. At a pressure difference of 500 Pa, the amount of water infiltrating through the specimen with defect (1.15%) was more than double of the amount infiltrating through the specimen without any defect (0.40%). Ullet and Brown [115] also performed cyclic tests at a mean pressure of 300 Pa and amplitude of 200 Pa with open vents in the EIFS. The presence of the vents in the EIFS, small air cavities in the grooves of the EPS and an air barrier at the interior side, ensured a reduced pressure difference over the EIFS, resulting in lower infiltration rates. Only a small increase in the infiltration rates was measured when air leakage openings were present in the air barrier.

More recently, Molnar et al. [116] conducted a qualitative pilot study on water infiltration through a crack in an ETICS specimen. Water was imposed to the crack by means of rectangular plastic holder creating a hydrostatic pressure between 400 and 600 Pa. Water infiltrated through all the cracked specimens and was either drained along the render-insulation interface or was transported towards the interior along the joints between the insulation panels or at mechanical fasteners.

4.3 Stucco

A traditional hardcoat stucco is typically a three layer cementitious rendering either applied over a solid masonry wall or applied over a metal lath, building paper and sheathing. These stuccos absorb water that impinges onto the exterior surface and have a certain buffer capacity. Synthetic stuccos on the other hand, include fibers and synthetic acrylics to add strength and flexibility and are also more water repellent and thus keep out more rainwater at the exterior surface. Cracks may however, occur in the surface of the stucco creating potential pathways for infiltrating water [117], [118]. Typical paint finishes can be used to reduce the water absorptivity of the stucco. However, these paints are not able to span micro cracks [56]. Saber et al. [119] conducted measurements of the infiltration rates across a cracked stucco surface applied to a metal lath. No infiltration was measured without pressure difference, but the infiltration percentages increased for increasing pressure difference. The amount of infiltrating water also increased for increasing water spray rates. In contrast, percentagewise the largest infiltration percentages were measured for the lowest water spray rate. Ngudjiharto [90] performed field testing on stucco walls (without drainage cavity) including a window. Similar to the tested siding wall (see section 4.1), the stucco wall had a South East orientation and the exterior was exposed to naturally occurring weather events. The infiltrated water that drained in between the stucco and building paper was collected by a trough at the bottom of the wall. The maximum percentage of infiltrated water collected by the bottom trough averaged over a one-month period was 2.3% of the wind-driven rain load. It was observed that water primarily infiltrated along the window-wall interface although no intentional defects were present.

4.4 Masonry

Historically, masonry walls have already been used for a very long time and consist of for example stonework or mortared bricks. These walls rely on the buffer capacity of the stones or bricks to prevent rainwater from infiltrating through the assembly. During a rain event, the exterior surface absorbs rainwater and transports it further into the wall. Due to the thickness of historic walls, it was very unlikely that accumulation of rainwater over time reached the interior side throughout a year, as evaporation to the outside and inside typically balances the rain load. However, nowadays masonry walls such as mortared clay bricks or concrete blocks are much thinner resulting in possible infiltrations through the wall.

Kahangi Shahreza et al. [120] determined that during the first 3.5 hours of wetting at a spray rate of 2-3.8 L/m^2/h, between 76% and 92% of the water applied to the brick masonry surface was absorbed. The time to attain surface saturation and runoff of water onto the surface depends on the sorptivity of the masonry and the applied spray rate or the amount of wind driven rain on the exterior surface. Based on the relation obtained by Hall and Kalimeris [32], the surface of a masonry brick wall with a sorptivity of 0.3 mm/$min^{1/2}$ and a moderate spray rate of 5 L/h becomes saturated after 8 minutes whereas the surface of a wall with a sorptivity of 3 mm/$min^{1/2}$ becomes saturated after 13h for the same spray rate. A higher sorptivity allows faster moisture transport within the brick and thus results in a longer period of time before surface saturation occurs compared to bricks with a lower sorptivity which hold water to the surface for a longer period of time [121]. Only when the surface of the wall is completely saturated, impinging rainwater starts to runoff and a larger portion of water may reach cracks or deficiencies for example at building envelope interfaces.

In general, it is assumed that the pressure difference acting over wall assemblies is the main driving force for water infiltration. However, in case of masonry walls, significant infiltration rates are measured without any external pressure difference once saturation of the entire wall is reached (see Table A 4). Water running off the exterior surface of the façade may be drawn in small cracks by capillary suction. Taking into account that the size of cracks is generally within the range of 0.1-1.0 mm and that the surface tension of water is approx. 0.075 N/m, the capillary suction pressure will be in the order of 75-750 Pa (for a contact angle of for example 60°). When water reaches the interior side of the brick, a meniscus is introduced due to surface tension which needs to be breached for infiltration to occur. The hydrostatic pressure created by the water flowing along the exterior surface and built up of water in the joints between the bricks, will cause the water in the cracks to flow out at the interior side of the masonry. In case of a vertical head joint of 60 mm, the hydrostatic pressure may reach 600 Pa which is enough to breach the meniscus in a crack of 0.125 mm wide [122].

Water infiltration primarily occurs at the interface between the brick and mortar at the vertical head joints [48], [120], [122], [123]. Chiovitti et al. [124] determined that once water starts to infiltrate and runoff at the interior side of the surface occurs, the relationship between the accumulated infiltrated water at the interior side and the elapsed time is quasi-linear. Hens et al. [123] confirmed this finding. If the pressure difference over the masonry is increased, the water infiltration rate also increases [48], [125]. Rathbone [125] additionally determined an increase in infiltration rate for an increased water spray rate. However, at a certain spray rate, the rate of increase decreased and in some cases, this leads to a maximum infiltration rate at a specific spray rate. For most specimens the maximum infiltration rate was reached at a spray rate of 1.25 L/min.m^2. This phenomenon can be explained by the fact that at higher spray rates, a uniform water film will be running off the exterior surface of the masonry. Increasing the spray rate will increase the thickness of the runoff film. Due to the increase in film thickness and the higher spray rate, the relative amount of waterdrops splashing open and bouncing of the exterior surface will also increase, resulting in a relatively lower amount of water available to infiltrate [22], [29]. Additionally, at a certain spray rate, the maximum amount of water able to infiltrate through the present deficiencies will be reached, resulting in a constant infiltration rate for increasing spray rates.

Due to the dependency of the infiltration rates on the spray rates and the applied pressure differences, the measured infiltration rates were also affected by the applied test method. Calle et al. [48] determined that the infiltration rates at a given mean pressure during cyclic testing were lower compared to the rates obtained during static testing. Due to the applied pulses (0-300 Pa), continuous water infiltration is interrupted resulting in lower total infiltration rates. Rathbone [125] found that the ranking order of the performance of the tested specimens with regard to the percentage of wetted area and the infiltration rate was the same for intermittent spray testing and continuous spray testing. However, the differences in performance of the specimens were a lot smaller for intermittent spraying than for continuous spraying.

Other factors affecting the infiltration rates through masonry walls are workmanship, the thickness of the walls and the properties of the materials (bricks, blocks, mortar, glue). Workmanship has a significant impact on the infiltration rates as rainwater may be transported easily through cracks towards the interior surface of the masonry. Calle et al. [48] measured an increase of the infiltration rate of 94% for a mortared brick specimen with cracks and poor workmanship relative to a specimen with normal workmanship. On the other hand Calle [126] measured a significant decrease of the infiltration rate for triple wythe masonries relative to single and double wythe masonries. Single and double wythe masonries showed infiltration rates in the same order of magnitude as continuous pathways (cracks at the mortar brick interface) were available for water to infiltrate. For triple wythe masonries however, only discontinuous pathways were present which resulted in a significant decrease of the infiltration rate, i.e. 1.30% of the spray rate compared to 21% of the spray rate, as well as a significant increase of the time to reach saturation of the whole surface, 360 minutes compared to 48 minutes.

Hens et al. [123] observed that larger infiltration rates were measured for more air permeable specimens. 0.64% of the applied spray rate infiltrated through discontinuous blocks with an air flow of 1.41 $m^3/h.m^2$ at 10 Pa, whereas only 0.08% of the spray rate infiltrated through continuous blocks with an air flow of 0.59 $m^3/h.m^2$ at 10 Pa. The larger airflow through the discontinuous blocks compared to the continuous blocks may be related to poor workmanship resulting in cracks between the blocks and mortar joints and voids in the mortar which in turn result in an increased number of leakage paths for water to infiltrate.

As most of the infiltrations are observed at vertical head joints, it is evident that the manner in which these joints are sealed affects the infiltration rates. Calle [126] observed that masonries with cement mortar are less watertight than masonries with lime mortar. Pointing mortars on the other hand, increase the watertightness of the masonries. Hens et al. [123] compared the water infiltration rates through mortared concrete blocks with the infiltration rates through glued concrete blocks with open head joints. During the laboratory tests, a significantly larger percentage of water infiltrated through the glued concrete blocks compared to the mortared blocks, i.e. averagely 70% of the spray rate infiltrated through glued concrete blocks compared to 0.39% of the spray rate through mortared blocks. However, during the field tests, smaller infiltration rates were measured for the glued masonries compared to the mortared masonries, in sheer contrast with the results of the laboratory tests. The maximum percentage of water infiltrating through the glued concrete blocks was 0.82% during the field tests compared to 3.37% for mortared concrete blocks. In the laboratory, an air permeable PMMA panel was applied at the interior side of the masonry, whereas in the field an airtight inner wall was positioned at the interior side. Combined with the open head joints of the glued masonry, the airtight inner wall reduced the pressure acting over the masonry. The mortared masonries on the other hand, only allowed a limited reduction of the pressure difference. As discussed above, a larger pressure difference results in larger infiltration rates. Hence, larger infiltration rates were measured through the mortared bricks compared to the glued bricks during the field tests.

The application of a clear water repellent coating can reduce the initial infiltration percentage after application. The coating provides a nanometric hydrophobic layer on the outer pore walls of the masonry to prevent infiltration of rainwater in the pore network. Brown [127] measured a reduction of the infiltration rate of 64% and 96% for clay bricks and concrete blocks respectively when treated with a clear water repellent coating. However, Chiovitti et al. [124] observed an increase in the infiltration rate through masonry treated with a clear water repellent coating over time, which indicates that the coating should be reapplied after a given time interval. Lubelli et al. [128] also observed that microcracks in the water repellent coating may occur due to dynamic solicitations on the masonry which results in water infiltration in the masonry and a reduced drying capacity of the wall towards the exterior. More research in this field is necessary to prove the long-term impact of water repellent coatings on the infiltration rates through masonry.

It should be noted that most of the reported infiltration percentages through masonry walls are obtained after several hours of testing and at extremely high water spray rates and wind pressures. Hens et al. [123] reduced the applied spray rate and pressure difference to respectively 0.5 – 0.6 L/min.m^2 and 25 Pa. Also Shahreza et al. [120] applied a reduced spray rate of 0.03 – 0.06 L/min.m^2 and no pressure difference, resulting in no water infiltration over a period of six cycles of 210 minutes of water spraying and 20 minutes of pausing. After 5 cycles 90% of the interior surface area showed dampness but no water infiltration. However, for some locations in Europe or North-America, masonry walls can remain very wet for long periods of time when subjected to outdoor weather conditions due to low solar radiation and high relative humidity [121].

4.5 Cladding panels with open joints

Facades with open joints consist of independent panels of for example fibre-cement, natural stone, wood, etc. These panels are typically installed on a wooden, steel or aluminium framework which is fastened onto the load-bearing wall. When rainwater hits the exterior surface, most of the raindrops will splash onto the surface or bounce back. A small portion may be absorbed by the panels depending on the absorptivity of the materials, and a relatively large portion of rainwater will infiltrate through the open joints between the panels. The forces that drive water through open joints are the kinetic energy of raindrops, gravity, pressure differences, local air currents, surface tension, hydrostatic pressures and capillary forces [129].

Recatala et al. [130] observed that the infiltration rates through open joints between fibre-cement panels remained constant for increasing pressure differences. Depending on the ratio of the area of openings in the air barrier (A_{ab}) to the area of openings in the exterior surface (A_{rs}), pressure equalization can be achieved [131]. According to Killip and Cheetham [132], 99% pressure equalization can be achieved when A_{rs} > 25-40 A_{ab}. As the ratio of A_{rs}/A_{ab} in the specimens of Recatala et al. [130] was more than 500, pressure equalization was achieved resulting in a highest measured pressure difference over the exterior cladding of 10 Pa for every pressure step (up to 750 Pa), even for the configuration with a poor airtightness (8.10 ± 0.27 m^3/h.m^2 at 50 Pa). This eliminates the pressure difference as one of the driving forces for water infiltration through the open joints. However, it should be noted that experimental assessments adopt a simplified approach that excludes air currents in the cavity between the pressurised and depressurised façades of a building. When the façade detailing does not include compartmentalisation at the corners of the building, these air currents may decrease the level of pressure equalisation, at the sides of the building.

The impact of the other driving forces, i.e. surface tension, hydrostatic pressure, capillary forces and gravity are primarily affected by the joint design. Mas et al. [40] determined infiltration percentages through joints between natural stone panels with both plane panel edges and non-plane panel edges for different joint widths. Panels with plane edges were panels with straight edges cut perpendicular to the panel surface resulting in a uniform joint width over the depth of the panels. Panels with non-plane edges had straight edges on two sides of the panels and two sides with a 5 mm deep groove cut out at the interior over half of the edge width, resulting in an increase of the joint width of 5 mm at the interior compared to the exterior. The latter joint profile introduces a small air gap within the joints and thus reduces the amount of water infiltrating due to surface tension and capillary action. In joints smaller than 8 mm, the non-plane edges resulted in lower infiltration percentages relative to the infiltration percentages through joints with plane edges. Whereas, for joints of 8 mm or larger, the effect of a non-plane edge was less significant. This implies that capillary action and surface tension are driving forces for water infiltration through joints smaller than 8 mm and gravity and kinetic energy of the raindrops are the main driving forces for water infiltration through joints of 8-10 mm and larger.

Recatala et al. [130] performed laboratory tests on fibre-cement panels with open joints of 10 mm and found a parabolic correlation between the spray rate and the rate of water infiltrating past the panels. For larger spray rates, on the one hand a larger amount of runoff is present at the surface covering the open joints and preventing wind-driven raindrops from entering, and on the other hand splashing of water drops increases when a water film is present on the surface [22]. This suggests that a maximum infiltration rate may be obtained for a given spray rate. This aligns with the conclusions drawn by Rathbone [125] for masonry walls.

Recatala et al. [133] also found that the more openings in the exterior surface are present (open joints and rivet holes), the more water infiltrates. The largest infiltration rates were found for panels riveted to top-hat profiles, suggesting that open vertical joints with additional capillary pathways between the panels and vertical profiles of the underlying frame promote relatively high infiltration rates.

On average 49,7% of the sprayed water splashed back, 22.5% created a runoff-film along the exterior surface and 27.8% infiltrated through the open joints [130]. It was also observed that most of the infiltrated water entered via the horizontal joints. When the horizontal joints were taped, only 0.7% of the sprayed water infiltrated, whereas 35% of the sprayed water infiltrated with taped vertical joints. In contrast, FVHF [134] reported that only 5.4% of sprayed water infiltrated through horizontal open joints of 8 mm, whereas 17% of sprayed water infiltrated through horizontal and vertical open joints of 8 mm. However, no details were reported on the test procedure, spraying system and subframe. Mas et al. [40] on the other hand, reported an infiltration percentage up to 45% of the spraying water for a joint of 8 mm and a panel thickness of 40 mm which is significantly larger than the infiltration percentages reported in other studies. Differences in the spraying system, i.e. spraying angle of the nozzles, spraying angle relative to vertical surface, distance to the panels and a larger spray rate may have caused differences in the infiltration percentage.

4.6 Curtain walls

Curtain walls either consist of vertical and horizontal framing members and infill material, i.e. stick systems, or prefabricated panels, i.e. unitized systems, which are installed onto the load-bearing building structure. The first curtain walls were constructed to keep out all rainwater. However, due to their complex geometry, water infiltration occurred. Therefore nowadays it is accepted that water will infiltrate through the exterior seal and drainage possibilities are provided before the infiltrated rainwater may reach the interior side of the curtain wall [135].

Although it is known that water infiltrates past the exterior seal, little to no information is available on the amount of water that infiltrates and thus needs to be drained. Therefore, Van Den Bossche et al. [51] conducted an experimental study, providing infiltration rates for an aluminium stick system curtain wall including a turn-and-tilt window. At the bottom of each vertical frame member (mullion) the infiltrated water behind the exterior seal was collected and weighed.

The results showed that there was only a slight increase in the infiltration rates for increasing pressure difference. It was observed that even at higher pressure, the pressure equalization percentage remained constant at 98%, resulting in a moderate pressure difference over the exterior gasket, i.e. at an applied pressure of 900 Pa, the pressure difference over the exterior gasket was only 18 Pa. This implies that the pressure difference was almost eliminated as a driving force for water infiltration and the hydrostatic pressure due to impinging raindrops or running off water caused water to infiltrate. In general, the infiltration rates were higher during cyclic testing than during static testing. During the cyclic test, rapid pressure pulses are applied which result in a time lag of the pressure in the curtain wall system, resulting in a higher pressure difference over the exterior seal and therefore higher infiltration rates.

5. Infiltration rates through joints at façade details

Joints at facade details leak. Even without the presence of perceivable deficiencies, water leakages may occur at interface details, primarily at window-wall interfaces. Olsson [136] determined that the amount of water leakages through interfaces which were built in laboratory conditions in the best possible way were not less than through interfaces with intentional deficiencies. One should therefore consider that deficiencies will be present through which water may leak if there are forces driving water through the openings. In case the exterior surface of the wall assembly has a low absorptivity or in case the exterior surface of a wall assembly with high absorptivity is completely saturated, relatively large amounts of rainwater will run off the exterior surface and may reach deficiencies at interface details. Olsson [65], [136] reported that out of 110 tested walls incorporating façade details in Sweden, 70% showed water leakages through the window-wall interface, independent of the wall type. Lacasse et al. [137] also concluded that water leakages occurred at window-wall interfaces regardless of the type of wall assembly.

Field measurements [65] showed that leakages occur at relatively low wind speed, i.e. 5-12 m/s and with a horizontal rain intensity of typically 2-3 mm/h, combined with wind-direction toward the leaking facades. Similar results were found in laboratory studies as most window-wall interfaces including deficiencies showed infiltration without or at relatively low pressure differences over the wall assembly (see Table A 8). This implies that other forces such as gravity, surface tension and capillarity are able to drive rainwater running off the façade through deficiencies at the interface. This may occur in particular at the lower corners of the window and the window sill. Increasing the pressure difference over the wall assembly did not necessarily result in larger infiltration rates. Sahal and Lacasse [138] also found that reducing the airtightness of the air barrier, resulting in an increased pressure difference over the cladding, only slightly increased the infiltration rates and percentages. The reverse phenomenon was also apparent as the addition of an air barrier lowering the pressure difference over the exterior seal, resulted in a decrease of the infiltration rate but did not eliminate infiltration [139].

Sahal and Lacasse [138] measured the infiltration rates through a defect at the window-wall interface of hardboard siding clad wall specimens for both water spraying onto the specimen and a water cascade at different spray rates. Water that infiltrated through the defect was collected by means of troughs located in the cavity underneath the window and at the base of the wall specimen. They found that in general, a water cascade resulted in higher infiltration rates compared to water spraying. The water film acted as a barrier in front of the deficiency reducing the airflow and thus increasing the pressure difference acting as a driving force. Increasing the cascade rate resulted in an increase of the infiltration rates but a decrease of the infiltration percentage. The increased rate increased the film thickness and in turn increased the pressure difference over the deficiency and the infiltration rates.

Ngudjiharto [90] performed a field study on window-wall interfaces in direct-fixed vinyl and stucco walls. The wind-driven rain amount was determined to be the primary factor affecting the infiltration rates. Infiltration percentages of 0,55% and 1,55% were measured for the vinyl and stucco wall respectively (WDR intensity between 0 and 2.5 L/m^2 and wind speed between 1-2 m/s). The reviewed laboratory studies reported infiltration percentages without pressure difference between 0-5.94% and at the highest measured pressure difference (200-600 Pa) between 0-8.13% relative to the spray rate per square meter. Infiltration through the deficiency occurred continuously or intermittently depending on the amount of water present at the deficiency [136], [140]. The observed infiltrations provided a concentrated flow of water at the point of the deficiency rather than a distributed load over the interior side of the wall.

In all of the reviewed studies, sealant was applied to seal the window-wall interface. It is acknowledged by the industry that deficiencies will occur in sealants over the lifespan of buildings [141]. A survey conducted in 1990 in the UK [142] reported that 55% of all examined building joints sealed with sealant had failed within 10 years and that only 15% did not show any evidence of leakage for more than 20 years. This underlines the importance of investigating the risk of water infiltration through deficiencies in sealants as well as the evaluation and development of alternative materials to seal window-wall interfaces. However, only Lacasse et al. [139] reported infiltration rates for a window-wall interface sealed by means of a rubber gasket, resulting in lower infiltration percentages, i.e. 2.12% of the spray rate compared with 3,18% for sealant at a pressure difference of 200 Pa.

Also at other façade details, for example ventilation ducts, electrical outlets or linear joints, deficiencies might be present through which water can infiltrate. Similar conclusions can be made for the infiltrations rates through deficiencies at ventilation ducts and electrical outlets as for the window-wall interfaces concerning the dependency of the infiltration rates on the pressure difference and the spray rate [137].

Lacasse et al. [143] conducted an extensive study on infiltration rates through cracks in sealed horizontal and vertical joints with and without displacement of the joint. Infiltration rates were measured for cracks with a length of 2-16 mm in sealed joints with a width of 20 mm. In the vertical joint, the crack was located at the side of the joint. In the horizontal joint, the crack was located at the bottom. In general, the water infiltration rates increased for increasing pressure difference and increasing water spray rate. Without pressure difference, only the vertical joints with cracks of 8-16 mm and a joint displacement of 2 mm showed infiltration, whereas no infiltration occurred through the other tested joints. At higher pressure differences however, infiltration occurred through all the tested vertical joints even without an extension of the joint width. It was observed that in general, higher infiltration percentages were obtained for vertical joints than for horizontal joints, i.e. for 81% of the data points vertical joints showed higher infiltration rates than horizontal joints. However, at large crack openings with a length of 8 – 16 mm and a displacement of 2 mm the infiltration percentages were higher for horizontal joints than for vertical joints, i.e. 2.63-3.48% compared with 0.24-0.30% respectively.

It should be noted that the infiltration percentages in Table A 8, Table A 9, Table A 10, Table A 11 are calculated relative to the spray rate per square meter. It would be more correct to relate the infiltration rate to the amount of water deposited onto the area above the deficiency or the façade detail. However, due to lack of information on the specific dimensions of the specimens this was not possible. Nonetheless, this would still be an approximation as not all the water deposited above the deficiency will flow along it or in contrast water deposited aside of the deficiency may reach it depending on the flow path of the water.

6. Discussion

6.1 Quantification of infiltration rates/percentages

In the reviewed studies, various types of cladding were subjected to wind simulated by an air pressure difference over the test specimen, either in a static or cyclic manner, and to rain either by spraying water directly onto the specimen or by water cascading down over the exterior surface. The total amount of water infiltrating through the exterior cladding surface, through defects in the cladding or defects at façade details, and reaching a drainage cavity, drainage material, weather-resistive barrier and/or materials that are not intended to get wet, were weighed and reported. The review showed that the dependency of the infiltration rates on the applied pressure difference and spray rate, was affected by the type of cladding and the present openings.

6.1.2 Impact of pressure difference

For increasing pressure difference applied over the test specimens, including the exterior cladding and in most cases an additional air barrier (see information provided in (Table A 1 - A 11), the infiltration percentage either increased or remained constant (Figure 2 and Figure 3). The infiltration percentage is defined as the total amount of water that infiltrated past the exterior cladding relative to the applied spray rate. A constant infiltration percentage for increasing pressure was observed for specimens which included a pressure equalized cavity reducing the pressure difference over the cladding. This was apparent for panel cladding with open joints and curtain walls. To obtain good pressure equalization (PEP > 90%) the airtightness of the air barrier should be at least ten times higher than the airtightness of the cladding [131]. The other cladding types as well as the deficiencies at façade details showed an increase of the infiltration percentage for increasing pressure difference.

The larger the openings in the exterior cladding surface, the smaller the pressure required for water to infiltrate and the higher the infiltration percentages. This was apparent for the panel cladding with open joints, the glued concrete blocks with open head joints and mortared masonry. Even without a pressure difference over the specimen, infiltration occurred. In reality, no pressure difference over a wall assembly, implies that there is no wind and therefore also no wind driven rain impinging the exterior surface of the assembly. However, water runoff may still occur depending on the geometry of the building causing a hydrostatic pressure onto the surface and possible infiltration through cracks or openings. The smaller the openings, cracks or deficiencies in the exterior surface or in case of concealed openings, the larger the pressure needs to be before infiltration occurs [41], which was apparent for sidings, ETICS and stucco. It should be noted that the infiltration percentages presented in Figure 2 for mortared masonry and glued concrete block were obtained for specimens which were subjected to several hours of water spraying which resulted in saturation of the specimens and relatively high infiltration rates as discussed in section 4.4.

When performing watertightness laboratory tests, it is recommended to measure the infiltration rate at several pressure steps between 0 Pa and 500 Pa or more, to obtain the most accurate results with regard to the correlation between the water infiltration percentages and the applied pressure difference. However, when it is preferred to limit the testing time, it is suggested to measure infiltration at 0 Pa, 300 Pa and 600 Pa, which can be considered a moderate and high pressure step respectively based on the determined parameters by Van Den Bossche [84]. The infiltration percentages at higher and intermediate pressure difference steps may be estimated by fitting a curve through the obtained data. The infiltration percentages reported in literature and shown in Figure 2 and Figure 3 suggest a linear increase of the infiltration percentage for increasing pressure difference. However, more data points are necessary for each cladding type to confirm this finding.

The infiltration percentages reported in Figure 2 and Figure 3 represent the total amount of water that infiltrated through the cladding of the evaluated test specimens. Evidently, when a cavity of more than 10 mm is present, only a portion of the infiltrated water reaches the interior side of the cavity. Water may reach the interior side of for example masonry cavity walls due to splashing on extruded mortar joints or water drops being transported along wall ties angled towards the interior. Calle [48] found that the ratio of water reaching the interior side of the cavity and the residual part of infiltrated water which in most cases drains along the interior side of the cladding, was dependent on the applied pressure difference. For increasing pressure difference, an increased portion of infiltrated water reached the interior side of the cavity. Ratios between 0.2% and 2.9% were found for pressure differences of 0 and 300 Pa respectively and a cavity width of 30 mm. For masonry walls with normal workmanship and a cavity width of 30 mm, of which the total infiltration percentage is reported in Figure 2, this results in 1.3% of the sprayed water reaching the interior side of the cavity and 45.3% being drained along the interior side of the cladding at a pressure difference of 300 Pa. Similarly, Recatala [130] reported that 0.5% of the sprayed water reached the interior side of a 100 mm cavity behind panel cladding with open joints and 27.3% either drained along the interior side of the cladding or drained in the cavity. None of the other studies differentiated between the percentage of water draining along the interior side of the cladding or reaching the interior side of the cavity. To conduct hygrothermal simulations from which to ascertain the water management of the facade, it is however, of importance to determine the portion of water that either drains along the interior side of the cladding or in the drainage cavity, or reaches the WRB or the interior side of the cavity. Besides the pressure difference, the portion of water crossing the cavity is also affected by the cavity width and whether water drops are able to infiltrate directly through large openings in the cladding in an unobstructed manner. For direct-fixed claddings, claddings with a clear cavity width smaller than 5 mm and deficiencies at interface details, it can be assumed that almost all infiltrated water will reach the material layer behind the cladding or interior side of the cavity. For claddings without open joints and clear cavity widths between 5 and 10 mm, it might be a safe approach to assume that 50% of the infiltrated rainwater will reach the interior side of the cavity. For cavity widths of 10 mm and larger, the largest portion of infiltrated water will drain along the interior side of the cladding. However, future research is necessary to provide more details on the percentage of water crossing the cavity and reaching the weather-resistive barrier for various claddings and cavity widths.

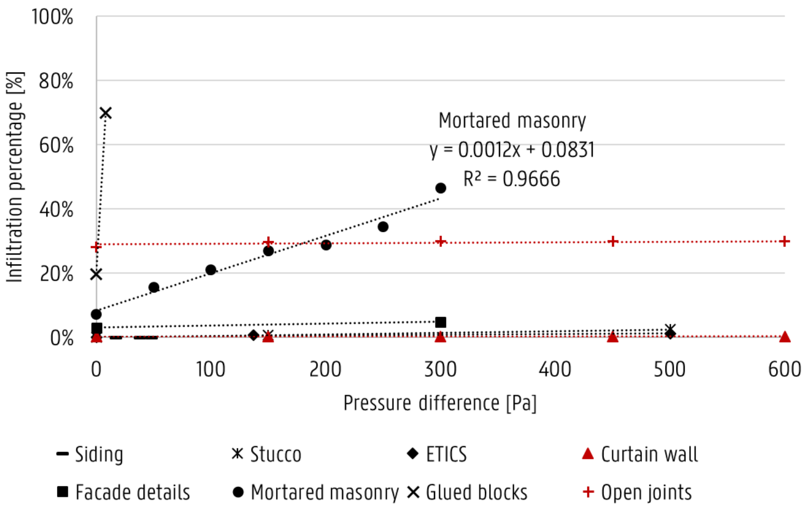

Figure 2: Infiltration percentages through siding with wedge defect [98], cracked stucco [119], ETICS with horizontal cut [115], curtain wall [51], deficiencies at facade details (average of results in [137]–[139], [144]), mortared masonry with normal workmanship [48], glued concrete (average of results glued concrete blocks in [123]) and panel claddings with open joints [130] relative to the applied pressure difference over the test specimens

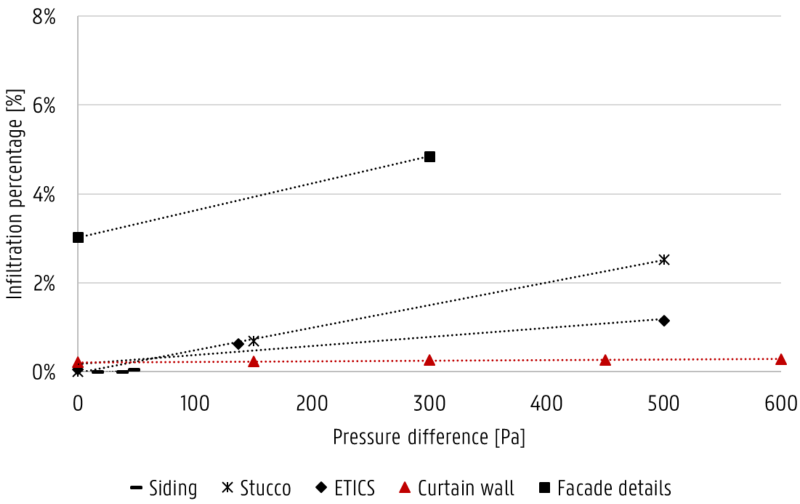

Figure 3: Detailed graph of infiltration percentages through siding with wedge defect [98], cracked stucco [119], ETICS with horizontal cut [115], curtain wall [51], deficiencies at facade details (average of results in [137]–[139], [144]) relative to the applied pressure difference over the test specimens

6.1.3 Static versus cyclic testing

Differences in infiltration percentages were measured during cyclic and static tests. Table 2 provides an overview of the reported static pressure difference steps per cladding type and mean cyclic pressure difference steps with corresponding amplitude. The infiltration percentage at a static pressure difference of for example 300 Pa is compared with the infiltration percentage at a mean pressure of 300 Pa during the cyclic test.

Table 2: Overview of reported static pressure difference steps and cyclic mean pressure difference steps with amplitude

Masonry and curtain wall		ETICS		Façade details	
Static (Pa)	Cyclic (Pa)	Static (Pa)	Cyclic (Pa)	Static (Pa)	Cyclic (Pa)
0	0	0	300 ± 200	0	
150	75 ± 75	137		75	75 ± 40
300	150 ± 150	500		150	150 ± 60
450	225 ± 225			300	300 ± 125
600	300 ± 300			600	700 ± 300

For the evaluated ETICS, mortared masonry specimens and deficiencies at façade details, the static pressure test resulted in larger infiltration percentages compared to the cyclic pressure test (Figure 4 and Figure 5). In contrast, the curtain wall specimen showed larger infiltration percentages during the cyclic test than during the static test. Although the infiltration percentages of both tests are compared for the same mean pressure, the momentarily lowered pressure during the cyclic test interrupted constant infiltration which resulted in lower infiltration percentages. The momentarily increased pressure during the cyclic test apparently does not compensate for the momentarily lowered pressure. In contrast, the infiltration through the curtain wall was not dependent on the pressure difference as good pressure equalization was achieved during the static test. During the cyclic test however, there was a time lag of the pressure in the cavity resulting in a lower pressure equalization at the onset of every cycle, resulting in higher infiltration rates. Note that this effect can only occur for configurations with a high vent ratio (volume of drainage space divided by the sum of effective cross-sections of the openings in the rainscreen).

In case it is preferred to only perform one watertightness test, a static pressure test should be chosen over a cyclic test, except when good pressure equalization is expected for a system with a high vent ratio.

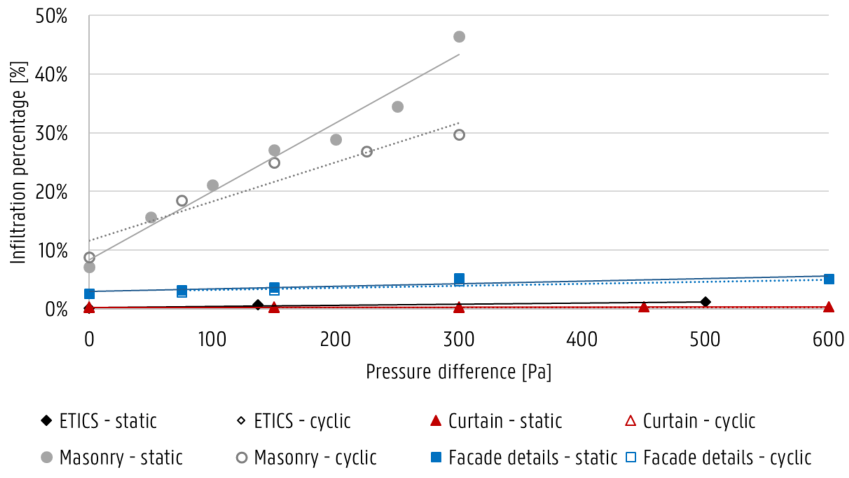

Figure 4: Infiltration percentages obtained during static and cyclic testing of ETICS with horizontal cut [115], curtain walls [51], mortared masonry with normal workmanship [48]and deficiencies at facade details (average of results for round and circular ducts in [137]) relative to the applied pressure difference

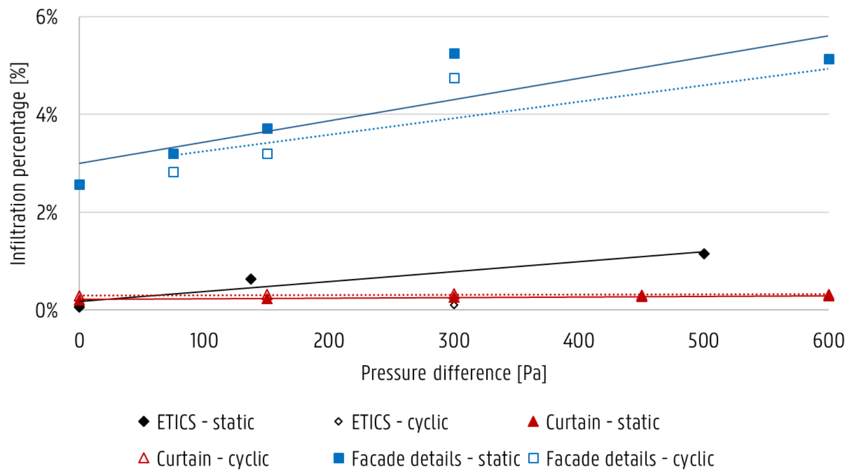

Figure 5: Detailed graph of infiltration percentages obtained during static and cyclic testing of ETICS with horizontal cut [115], curtain walls [51] and deficiencies at facade details (average of results for round and circular ducts in [137]) relative to the applied pressure difference

6.1.4 Impact of spray rate

In general, an increased spray rate resulted in higher infiltration rates (Figure 6 and Figure 7 left). The largest increase in infiltration rate relative to the spray rate was observed through the open joints between the panel cladding. Percentagewise, the infiltrated portion through the open joints relative to the spray rate remained constant for increasing spray rate, whereas the infiltration percentage through stucco and mortared masonry decreased for increasing spray rate (Figure 6 and Figure 7 right). In general, a higher spray rate results in a thicker runoff film and a larger percentage of waterdrops splashing and bouncing of the exterior surface, reducing the relative amount of water available to infiltrate [22]. This phenomenon will be apparent at lower spray rates for exterior cladding surfaces without large openings compared to exterior surfaces with open joints. It is assumed that the relative impact of the kinetic energy of the waterdrops flowing directly through the open joints nullifies the effect of increased splashing and bouncing of drops.

A percentagewise decrease for increasing spray rate was also observed for deficiencies at façade details when water cascaded down the exterior surface (Figure 7 right) [138]. When water cascaded down the exterior surface, no splashing and bouncing of drops occurred. On the other hand, for increasing cascading rates, the thickness of the runoff film increased which in turn increased the pressure difference acting over the deficiency by reducing the airflow through the opening and thus increased the infiltration rate. It is however, hypothesized that a maximum amount of water may infiltrate through an opening for a given pressure difference, which resulted in a decrease of the infiltration percentage for increasing spray rate. The larger the openings, the larger the maximum infiltration rate.

Additionally, for increased cascading rates, the thickness of runoff rivulets increases up to a maximum film thickness. When the maximum film thickness is reached, the rivulet becomes wider which may result in a uniform film flowing over a larger surface area. This increases the likelihood of water reaching deficiencies through which infiltration may occur up to the point where a full uniform film flow is reached over the entire surface but does not necessarily increases the amount of water available to infiltrate at a deficiency to the same extent, resulting in a decreased percentage of infiltrated water [145].

Due to the stochastic nature of water running off a test specimen when water is sprayed, it might be possible that more or less water reaches a deficiency during one test than during another test. This may result in an increase or decrease of the infiltration rate and infiltration percentage for increasing spray rates at a specific pressure step, independent of the increased spray rate. This resulted in the lack of a clear relation between the infiltration rate or percentage and the spray rate for both the deficiencies at façade details evaluated by means of water spraying onto the specimen and deficiencies at window-wall interfaces (Figure 7 façade details – spray and window-wall interface). To accurately predict the infiltration rate through deficiencies, it is recommended to either ensure that a runoff film is present over the openings by limiting the distance between the direct impinging spray and the deficiency location, to extend the test time ensuring that the infiltration rate can be averaged over a longer period or to repeat the tests at least three times and reporting the average values and the spreading on the results.

A second order polynomial curve shows the best fit through the infiltration rates of the stucco and masonry specimen and the specimen with deficiencies at façade details (cascading water) (Figure 6 and 7). When the intercept is set to zero, no infiltration occurs without water spraying, the stucco and masonry specimen show a maximum infiltration rate at 3.2 and 1.4 L/min.m^2 respectively at a pressure difference of 500 Pa and 3.6 and 1.4 L/min.m^2 at a pressure difference of 150 Pa. For stucco and mortared masonry, a spray rate of 3,4 L/min.m^2 which is commonly used in North America may thus be considered as a conservative value to evaluate the infiltration rate. For claddings with deficiencies, the maximum is only reached at higher spray rates, for example at a spray rate of 5.1 L/min.m^2 through a 50 mm deficiency at façade details at a pressure difference of 300 Pa. Taken into account that 2 L/min.m^2 and 3,4 L/min.m^2 can already be considered as high rain intensities in a Belgian and North American context respectively and the fact that the relative portion of infiltrated water decreases for increasing spray rate or only slightly increases, a spray rate of 3.4 L/min.m^2 may be considered as conservative in general.

As previously mentioned, the increased amount of waterdrops flowing directly through the open joints due to their kinetic energy nullifies the effect of increased splashing and bouncing of drops on facades with open joints due to an increase in spray rate. This results in a linear increase of the infiltration rate for increasing spray rate and a constant infiltration percentage (Figure 6). However, more data points are necessary for each cladding type to confirm these relations.

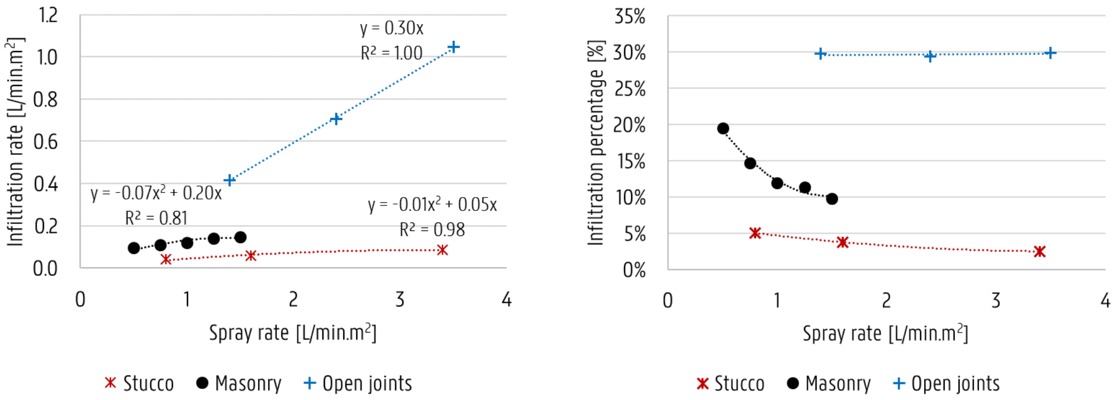

Figure 6: Infiltration rates (left) and percentages (right) through cracked stucco [119], mortared concrete masonry with good workmanship [125]and panel cladding with open joints [130] relative to the applied spray rate

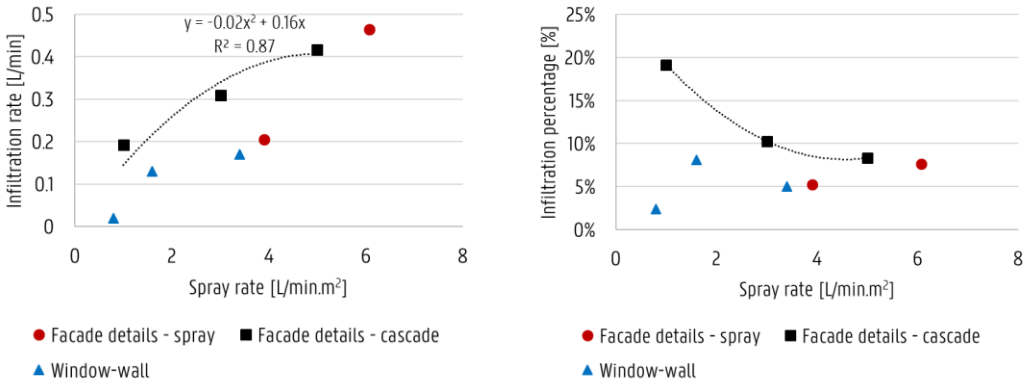

Figure 7: Infiltration rates (left) and percentages (right) through deficiencies at facade details for water spraying (average of results for circular and rectangular ducts in [137]) and cascading (average of results for circular and rectangular ducts in [138]) down the exterior surface and window-wall interface [144] relative to the applied spray rate

6.2 Water entry functions

To perform hygrothermal simulations including the full water management of the wall configuration, a moisture load should be defined representing the infiltrated water in a wall assembly. The previously reported studies showed that the infiltration rates and percentages are dependent on the applied spray rate and pressure difference over the wall assembly and thus in reality on the wind-driven rain (WDR) and driving rain wind pressure (DRWP). As the WDR and DRWP values vary over time and for different locations, it is essential to provide a water entry function as moisture load which includes the combined effect of WDR (or spray rate) and DRWP (or pressure difference).

Sahal and Lacasse [138] established a water entry function based on infiltration rates in the stud cavity of hardboard siding-clad walls. They derived a linear function that relates the water entry rate Q (L/min) to the spray rate R_p (L/min.m^2) for each static pressure difference ΔP (Pa):

$$Q = m_p * R_p \qquad (3)$$

Where: Q is the water entry rate (L/min), R_p is the spray rate (L/min.m^2) and m_p is the water entry potential (L min^{-1}/l min^{-1} m^{-2}). The water entry potential m_p is an empirical function and was derived for the ventilation duct of the hardboard siding-clad wall by fitting a third order polynomial curve to the data:

$$m_p = 3*10^{-11}(\Delta P)^3 - 8*10^{-7}(\Delta P)^2 + 5*10^{-5}(\Delta P) + 0.0123 \qquad (4)$$

In contrast with what is presented by Sahal and Lacasse, the reviewed studies in this paper showed a non-linear relation between the water infiltration rate and the spray rate and a maximum infiltration rate for a certain spray rate.

Moore et al. [146] also derived a water entry function to calculate the water entry for a given quantity of *WDR* and wind-induced pressure (P):

$$WE=WDR*WE\% \qquad (5)$$

Where *WDR* is wind-driven rain (L/h.m^2), *WE* is water entry (L/h.m^2) and *WE%* is the percentage of water entry for each cladding type (decimal form). The percentage of water entry for any given cladding type is given by a power function:

$$WE\%=a*P^b \qquad (6)$$

Where *a* and *b* are fitting factors and *P* is the wind-induced pressure (Pa). The factors *a* and *b* are derived by fitting a power function to the results obtained from watertightness tests averaged for different spray rates. Hence, the specific impact of a varying spray rate or varying WDR is not given by these relations. Additionally, the power function relating the water entry percentage to the pressure implies that no water entry occurs at zero wind-induced pressure, whereas the reviewed studies showed that water entry occurred without any induced wind-pressure.

Xiao et al. [147], [148] provide a two-step approach to derive a water entry function. The first step consists in determining the coefficients α and β which represent the relative impact of the wind-driven rain (*WDR*) and driving rain wind pressure (*DRWP*). The *WDRP Index* (WDRPI) is defined to determine the combined effect of both *WDR* and *DRWP*:

$$WDRP\ Index= WDR^{\alpha}*DRWP^{\beta} \qquad (7)$$

Values for α and β were determined by correlating the *WDRPI* to measured infiltration rates through deficiencies in a vinyl-clad wall under dynamic pressure differences for different spray rates and pressure steps. The second step in the proposed approach consists of determining the water entry rate from the *WDRPI* and coefficients *a* and *b* by means of a power function:

$$WE=a*WDRPI^b \qquad (8)$$

The coefficients *a* and *b* were determined by the least-square method and their respective values for the vinyl-clad wall assembly. Although a methodology to include the effect of both the spray rate and the pressure difference is provided by this approach, it also assumes no water infiltration without wind-induced pressure and does not take into account a maximum infiltration rate for a given water spray rate and pressure difference.

Although the presented water entry functions do not take into account every aspect of the dependency of water infiltration on the pressure difference and water spray rate, they provide a valuable base for further improvement of the definition of water entry functions for different cladding types. Further quantitative research on the infiltration rates for different spray rates and pressure difference steps is, however, necessary to increase the accuracy of these functions and to define the relation between water infiltration, spray rate or wind-driven rain and pressure difference or driving rain wind pressure more precisely.

The water entry functions provide a basis to implement water ingress in hygrothermal simulations. This is typically done by implementing a moisture source in numerical simulation models, and more specifically by adopting a fraction of the WDR as moisture load in one or more cells of the configuration. It should be noted that to the knowledge of the authors, no simulation models exist that explicitly account for the effect of drainage inside building components. However, when water is supplied by the source term to one or more grid cells in subsequent time steps, very often the supply exceeds the redistribution rate within the construction. That may cause a very quick increase in the moisture content of those cells, often well above the open porosity of the material which is physically not possible. Hence, these models have implicit or explicit cut-off values that prevent the moisture content to rise above a certain threshold value, and hence the moisture source is by default removed from the moisture balance in the model. By consequence, this effect can also be used by the modeler to implement the effect of drainage in a wall assembly, and in some cases it can even be advisable to split up materials layers and change for example the open porosity to accommodate implementing the source term in a realistic way. When implementing water ingress in hygrothermal simulations by means of water entry functions, it is important to consider how the simulation model implements this in the model. Whenever a source term is implemented in a hygrothermal model, it is key to evaluate what exactly happens in the model, to what extent moisture is in fact removed out of the equation as explained above, and to what extent drainage occurs in reality. Finally, it should be noted that these results are highly sensitive to the location, material, and number of grid cells in which the source term is implemented.

6.3 Categorization of exterior cladding surfaces

The previously mentioned water entry functions may be used as input for hygrothermal simulations. However, to obtain these water entry functions it is necessary to conduct laboratory tests at different spray rates and pressure levels. These tests are not available for every type of cladding and façade detail and it is not always preferable to conduct new tests when a building is designed. ASHRAE Standard 160 [78] therefore, proposed a default infiltration rate of 1%. However, based on the presented review it is clear that infiltration percentages differ for different cladding types and that 1% is not always a reasonable assumption.

To gain insight in the expected infiltration percentages for a cladding type during the design phase, without performing additional laboratory studies, a categorization of exterior cladding surfaces is developed (Figure 9).

The initial categorization is whether the cladding surface is continuous or discontinuous:

- A continuous cladding system does not include joints between different cladding elements, not taken into account joints at façade details such as windows or ducts. At the exterior, these claddings are perceived as a continuous surface. Water infiltration through continuous cladding systems is most likely to occur through cracks in the surface.
- A discontinuous cladding system does include joints between different cladding elements. These elements may for example be blocks, panels or boards, which are either stacked one onto the other or attached to a substructure. Water infiltration is most likely to occur through the present joints, in particular at the interface between the joint and the substrate.

The discontinuous cladding systems are further subdivided with regard to the type of joints that are present (Figure 8):

- Lap joints: an overlap is present between the different cladding elements. Lap joints may be present in different ways, for example one element is applied on top of the other element in an overlapping manner or two elements are connected with shiplap joints. There are no openings that provide a direct horizontal path for infiltrating water towards the interior. Water infiltration is most likely to occur through deficiencies in the lap joint by capillary action.
- Sealed joints: all joints between the cladding elements are sealed by means of for example mortar, elastomeric sealant, foam sealing tape, etc. Water infiltration is most likely to occur through deficiencies at the interface between the joint sealing material and the substrate.
- Open joints: either horizontal, vertical or all joints between cladding elements are open providing a direct path for water to infiltrate. Open joints may either be present between panels or blocks. Blocks are defined as elements which have a thickness that is within the same order of magnitude as either the width or height of

the elements. Vice versa panels are defined as elements with a thickness several times smaller than the width or height of the elements. It is assumed that the total length of joints of facades composed of blocks will be several times larger than the total length of joints between panels.

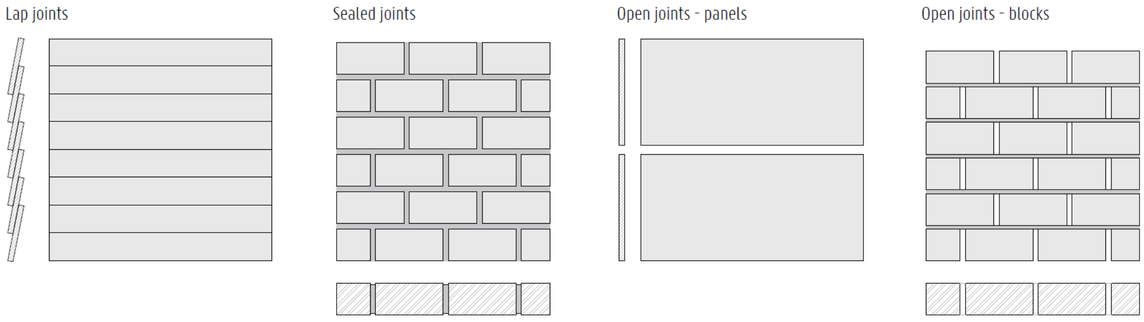

Figure 8: Cross-sections and front views of discontinuous exterior claddings with lap joints, sealed joints and open joints between panels and blocks

Discontinuous exterior cladding surfaces with lap joints and sealed joints are further subdivided based on the pressure equalization potential of the wall assembly. High pressure equalization (PE) is considered when the pressure equalization potential is more than 90% which may be achieved when the airtightness of the air barrier is at least ten times higher than the airtightness of the cladding [131]. A high pressure equalization will result in less infiltration as the pressure difference is reduced as a driving force. It is assumed that the pressure equalization potential of continuous claddings will always be low as the number of intentional openings will be limited. In contrast, it is assumed that the pressure equalization potential for claddings with open joints will always be high.

The absorption characteristics of the materials could also be criteria to categorize claddings. Exterior cladding surfaces with high absorptive materials will slow down water infiltration through the cladding as water infiltrating through for example cracks will be first absorbed sideways by the materials before infiltration towards the interior occurs. Rainwater reaching cracks in non-absorptive materials on the other hand, will infiltrate immediately towards the interior when an external pressure is applied. However, no test results were available showing this difference in infiltration phenomenon as only tests were conducted for saturated absorptive materials which act similarly as non-absorptive materials. Future research should look into the absorption of infiltrated rainwater through for example cracks to be able to predict more precisely when infiltration will occur through claddings with absorptive materials.

Besides water infiltration through the exterior cladding surface, also infiltration at façade details should be taken into account. A categorisation is made based on the type of façade detail, i.e. window-wall interface, circular ducts, rectangular ducts and linear joints. Average infiltration percentages at façade details are also provided per cladding category, when available in literature.

For each category an example of cladding is given and when available, percentages of water infiltrating past the exterior cladding found in literature are reported (Figure 8). The infiltration percentages are given for two pressure difference steps which are defined between brackets as well as the spray rate. Additionally, references are indicated which provide more information on the infiltration rates.

(1) ETICS [115]
(2) Stucco [119]
(3) Vinyl siding [98]
(4) Curtain walls [51]
(5), (6), (7) Mortared bricks [124], [126], [127]
(8), (9), (6) Mortared concrete blocks [123], [125], [127]
(10) Fibre cement panels with open joints [133]
(11) Natural stone panels with open joints [40]
(12) Façade details for different claddings [137]
(13) Window-wall interface [144]
(14) Façade details for vinyl siding [138]
(15) Linear joints [143]

Future research should include watertightness tests for various cladding types to provide ranges of infiltration percentages that can be expected for each category. Ideally, a distribution of expected infiltration percentages should be provided for each category, as well as the location to which the infiltration percentages should be applied.

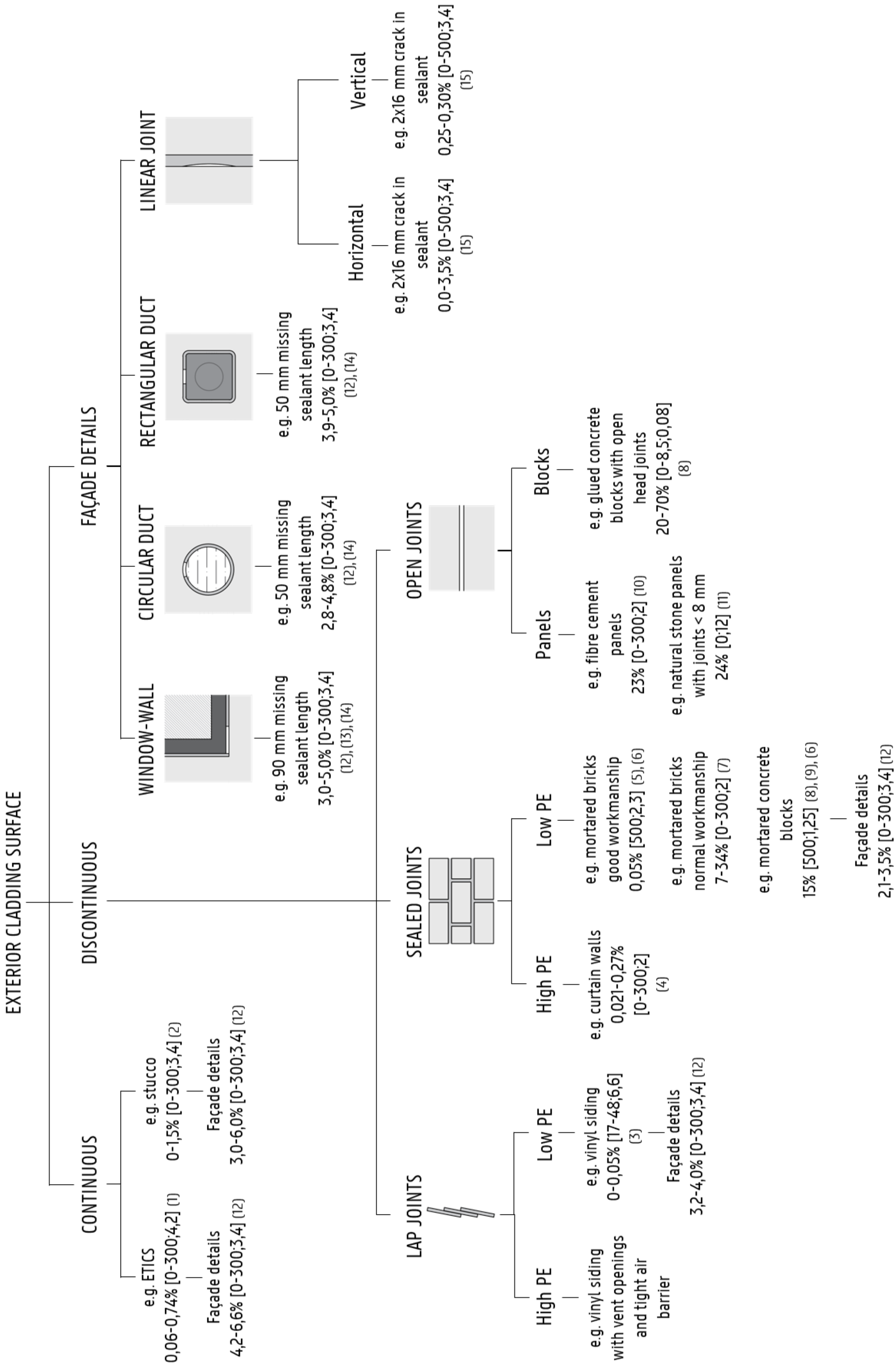

Figure 9: Categorization of exterior cladding surfaces and facade details based on water infiltration mode

7. Conclusions

Knowledge of infiltration rates in wall assemblies is of importance as they can affect and even dominate the water and moisture management. Quantitative data can be applied as input for hygrothermal simulations and as inlet flow rates for drainage tests to evaluate the behaviour of water in drainage cavities. Therefore a review of studies evaluating infiltration rates for different cladding types was presented.

Based on the analysis of the available results in literature, the following methodology is proposed to obtain information on infiltration rates based on the required specificity and available information:

1. Case-specific: when detailed knowledge on the infiltration rates is required for a specific wall assembly it is recommended to perform watertightness tests in the laboratory on a mock-up simulating part of the specific wall assembly. The mock-up should include an air barrier at the interior side with a conservative airtightness to reduce the impact of pressure equalization, providing a worst-case scenario.
    a. Most accurate results can be obtained when laboratory tests are conducted at multiple pressure difference steps and multiple spray rates. Differentiation should be made between infiltrated water that is drained along the interior side of the cladding, water that reaches the centre part of the cavity and/or is drained along the interior side of the cavity. Based on the results, a water entry function can be established which can be used as input to define the moisture load for varying wind-driven rain and driving rain wind pressure.
    b. In case it is preferred to limit the testing time, it is recommended to conduct watertightness tests at a spray rate of 2.0 L/min.m^2 or 3.4 L/min.m^2, in a European and North American context respectively, and at pressure difference steps of 0 Pa, 300 Pa and 600 Pa. These pressure difference steps will provide information on the potential infiltration without wind pressure, at a moderate and high pressure. Based on the obtained relation for the infiltration rates to the pressure difference and spray rate in this study, a polynomial curve of second order may be fitted through the results to predict infiltration rates at other spray rates and pressure differences.
2. Material-specific: when it is not preferred to conduct laboratory tests, information on infiltration rates for similar materials in literature may be used as input. For this purpose, a categorization scheme of exterior cladding surfaces has been developed based on the characteristics of claddings with regard to the infiltration mode.

3. Conceptual: when no specific information on the cladding materials is available but it is known whether the cladding consists of a continuous or discontinuous surface and in case of a discontinuous surface it is known what type of joints are present, a range of expected infiltration rates may be determined based on the categorization scheme.
4. Generic: when no information is available on the materials or cladding concept one can apply an infiltration percentage of 1% as proposed by ASHRAE Standard 160. It should however, be kept in mind that for certain cases this will lead to an underestimation of the infiltration rates, for example for panel cladding with open joints or mortared concrete blocks, or an overestimation, for example for vinyl siding.

Besides infiltration through the exterior cladding surface, it is also of importance to take into account infiltration through joints at façade details. At window-wall interfaces for example, infiltration percentages of 3-5% of the spray rate were measured at pressure difference of 0 Pa and 300 Pa through a 90 mm slit in the sealant.

Future research on watertightness of wall assemblies should focus on quantitative measurements of the infiltrated water through the exterior cladding surface differentiating between the water that infiltrates and drains along the interior side of the cladding or reaches the interior side of the cavity. These measurements will increase the accuracy of water entry functions and will provide more input for the categorization scheme which is a helpful tool to determine infiltration rates without performing laboratory tests.

Appendix

Table A 1: Water infiltration rates and percentages through sidings

Ref.	Materials	Specimen size (m^2)	Defect	Air barrier ($m^3/h.m^2$ @ 50 Pa)	Test procedure	Spray rate ($L/min.m^2$)	ΔP (Pa)	Infiltration (L/min) per pressure step ΔP (Pa)			Infiltration (%) per pressure step ΔP (Pa)		
								ΔP17	ΔP30	ΔP48	ΔP17	ΔP30	ΔP48
Boardman and Glass [98]	Vinyl lap siding	9.3	3 wedges slid up between the siding	OSB (-)	Static pressure	6.6	17-30-48	0.000	0.001	0.028	0.00%	0.001%	0.046%
						Monthly WDR	Wind speed	Monthly infiltration (l)			Monthly infiltration (%)		
Ngudjiharto [90]	Vinyl Dutch-lap siding	4.2	Unintentional defect at window-wall	PE-sheet and gypsum board (-)	Field test	30 mm	1-2 m/s	-	-	0.335	-	-	0.27%

Table A 2: Water infiltration rates and percentages through ETICS

Ref.	Materials	Specimen size (m^2)	Defect	Air barrier ($m^3/h.m^2$ @ 50 Pa)	Test procedure	Spray rate ($L/min.m^2$)	ΔP (Pa)	Infiltration (L/min) per pressure step ΔP (Pa)			Infiltration (%) per pressure step ΔP (Pa)		
								ΔP0	ΔP137	ΔP500	ΔP0	ΔP137	ΔP500
Ullet et al. [115]	3 mm coat over 50 mm EPS	2.9	Horizontal cut	Trowelled coating on gypsum board (0.20)	Static pressure	4.2	0-137-500	0.007	0.078	0.141	0.06%	0.63%	1.15%
			No defect					0.008	0.021	0.049	0.06%	0.17%	0.40%
								ΔP300 ± 200			ΔP300 ± 200		
			Horizontal cut	2.31	Dynamic pressure (open vent area)		300 ± 200	-	0.012	-	-	0.10%	-
				0.20				-	0.009	-	-	0.07%	-
			No defect	2.31				-	0.009	-	-	0.07%	-
				0.20				-	0.007	-	-	0.06%	-

Table A 3: Water infiltration rates and percentages through stucco

Ref.	Materials	Specimen size (m^2)	Defect	Air barrier ($m^3/h.m^2$ @ 50 Pa)	Test procedure	Spray rate ($L/min.m^2$)	ΔP (Pa)	Infiltration (L/min) per pressure step ΔP (Pa)			Infiltration (%) per pressure step ΔP (Pa)		
								ΔP0	ΔP150	ΔP500	ΔP0	ΔP150	ΔP500
Saber et al. [119]	NBC-compliant stucco	6.0	Un-intentional cracks	Not reported	Static pressure	0.8	0-150-500	0.000	0.070	0.240	0.00%	1.47%	5.04%
						1.6	0-150-500	0.000	0.085	0.360	0.00%	0.89%	3.78%
						3.4	0-150-500	0.000	0.140	0.510	0.00%	0.69%	2.52%
						Monthly WDR	Wind speed	Monthly infiltration (l)			Monthly infiltration (%)		
Ngudjiharto [90]	3 coat stucco acrylic finish	4,2	Un-intentional defect at window-wall	PE-sheet and gypsum board (-)	Field test	30 mm	1-2 m/s	-	-	2.9	-	-	2.30%

Table A 4: Water infiltration rates and percentages through brick masonry walls

Ref.	Materials	Specimen size (m^2)	Workmanship	Air barrier ($m^3/h.m^2$ @ 50 Pa)	Test procedure	Total duration (h)	Spray rate ($L/min.m^2$)	ΔP (Pa)	Infiltration ($L/min.m^2$) per pressure step ΔP (Pa)		Infiltration (%) per pressure step ΔP (Pa)	
									ΔP0	ΔP300	ΔP0	ΔP300
Calle et al. [48]	Bricks + cement mortar	0.71	Normal	PMMA (2,0)	NEN 2778 (static)	1.5	2	0-300	0.144	0.933	7.19%	46.64%
			Normal - cracks						0.302	0.651	15.11%	32.57%
			Poor						0.294	0.731	14.68%	36.54%
			Poor - cracks						0.419	1.808	20.96%	90.39%
									ΔP0	ΔP300	ΔP0	ΔP300

			Normal						0.176	0.500	8.78%	25.00%
			Normal - cracks		EN 12865 (cyclic)	1	2	0-300	0.119	0.410	5.96%	20.52%
			Poor						0.249	0.578	12.43%	28.88%
			Poor - cracks						0.725	0.993	36.27%	49.67%
									ΔP0	ΔP300	ΔP0	ΔP300
	Single wythe					1.5			0.120	0.420	6.00%	21.00%
Calle [126]	Double wythe	0.71	Normal	PMMA (2,0)	EN 1027 (static)	2	2	0-300	0.140	0.420	7.00%	21.00%
	Triple wythe					6.7			0.026	0.026	1.30%	1.30%
										ΔP500		ΔP500
Chiovitti et al. [124]	Uncoated	2.2	Good	No air barrier	ASTM E541 (static)	4	2.3	500	-	0.00009	-	0.004%
	Coated								-	0.00007	-	0.003%
										ΔP479		ΔP479
Brown [127]	Uncoated	1.5	Good	No air barrier	ASTM E514 (static)	24	2.3	479	-	0.0021	-	0.09%
	Coated								-	0.0007	-	0.03%
									ΔP0		ΔP0	
Shahreza et al. [120]	Clay brick + mix mortar	0.1	Good	-	-	23	0.033-0.06	0	0.000	-	0.00%	-

Table A 5: Water infiltration rates and percentages through masonry walls with concrete blocks

Ref.	Materials	Specimen size (m^2)	Work-manship	Air barrier ($m^3/h.m^2$ @ 50 Pa)	Test procedure	Total duration (h)	Spray rate ($L/min.m^2$)	ΔP (Pa)	Infiltration ($L/min.m^2$) per pressure step ΔP (Pa)		Infiltration (%) per pressure step ΔP (Pa)	
									ΔP0	ΔP25	ΔP0	ΔP25
	Continuous blocks								0.0003	0.0005	0.05%	0.08%
	Double layer blocks	0.9	Good	Air permeable PMMA (-)	Static	4-6	0.5-0.6	0-25	0.0000	0.0011	0.01%	0.22%
	Split blocks								0.0053	0.0042	1.04%	0.61%
	Discontinuous blocks								0.0437	0.0058	5.97%	0.64%
Hens et al. [123]									ΔP0	ΔP8.5	ΔP0	ΔP8.5
	Glued continuous blocks								0.0137	0.0528	13.55%	71.48%
	Glued double layer blocks								0.0578	0.0686	53.61%	85.73%
	Glued split blocks	0.9	Good	Air permeable PMMA (-)	Static	6	0.06-0.10	0-8.5	0.0094	0.0329	11.41%	52.31%
	Glued discontinuous blocks								0.00001	0.0497	0.01%	70.48%
										ΔP500		ΔP500
			Good				1.25		-	0.1910	-	15.28%
			Poor						-	0.3945	-	31.56%
							1.5		-	0.1475	-	9.83%
Rathbone [125]	Variable blocks	4		No air barrier	BS 4315 continuous spray	48-72	1.25	500	-	0.1425	-	11.40%
			Good				1		-	0.1200	-	12.00%
							0.75		-	0.1100	-	14.67%
							0.5		-	0.0975	-	19.50%
										ΔP479		ΔP479
Brown [127]	Uncoated	1.5	Good	No air barrier	ASTM E514 (static)	24	2.3	479	-	0.6508	-	27.89%
	Coated								-	0.0232	-	0.99%

Table A 6: Water infiltration rates and percentages through the open joints of cladding panels (V=vertical, H=horizontal)

Ref.	Materials	Specimen size (m^2)	Joint length (m)	Secondary structure	Joint width (mm)	Air barrier (m^3/h.m^2 @ 50 Pa)	Test procedure	Spray rate (L/min.m^2)	ΔP (Pa)	Inf. (L/min)	Inf. (L/min.m)	Inf. (%)
Recatala et al. [130]	Fibre cement (63 x 30 x 1.2 cm)	3.5	3.7 V + 9.55 H	Horizontal C-section on vertical T-profiles	10	PMMA (1,67)	EN 12155 (static)	1.4	0-300-750	1.46	0.110	29.7%
								2.4		2.47	0.186	29.4%
								3.5		3.66	0.276	29.9%
			3.7 V					2		0.046	0.0124	0.7%
			9.55 H					2		2.45	0.256	35.0%
Recatala et al. [133]	Fibre cement (34 x 100 x 0.8 cm)	3.9	10.5 V + 1.93 H	Vertical top-hat profiles	10	PMMA (1,67)	EN 12155 (static)	2	0-300-750	1.90	0.153	24.41%
	Fibre cement (63 x 30 x 1.2 cm)	3.5	3.7 V + 9.55 H	Horizontal C-section on vertical T-profiles						1.36	0.103	19.41%
		3.5	3.7 V + 9.55 H	Vertical T-profiles						1.42	0.107	20.35%
Mas et al. [40]	Stone (90 x 60 x 4 cm)	2.16	1.8 H + 1.2 V	-	4	No air barrier	EN 12155 (static)	12	0	3.1104	1.0368	12%
					6					9.3312	3.1104	36%
					8					11.664	3.888	45%
Fernandez Madrid [149]	-	1	Round	-	-	Panel with openings (3-12 cm^2)	Static	2.7	0-300-600	0.158	-	5.83%
FVHF [134]	(60 x 60 cm)	-	H	-	8	Not reported	-	-	-	-	-	5.4%
			H + V	-						-	-	17.0%

Table A 7: Water infiltration rates and infiltration percentages through the exterior seal of a stick system curtain wall tested by Van Den Bossche et al. [48]

Specimen size (m^2)	Air barrier (m^3/h.m^2 @ 50 Pa)	Test procedure	Spray rate (L/min.m^2)	ΔP (Pa)	Infiltration (L/min) per pressure step ΔP (Pa)			Infiltration (%) per pressure step ΔP (Pa)		
					ΔP0	ΔP300	ΔP600	ΔP0	ΔP300	ΔP600
12	0.44	EN 12155	2	0-300-600	0.05	0.064	0.069	0.21%	0.27%	0.29%
		EN 12865			0.07	0.079	0.077	0.29%	0.33%	0.32%

Table A 8: Water infiltration rates and percentages through window-wall interfaces

Ref.	Exterior surface	Sealing method	Deficiency type	Dimensions	Air barrier (m^3/h.m^2 @ 50 Pa)	Test procedure	Spray rate (L/min.m^2)	Infiltration (L/min) per pressure step ΔP (Pa)			Infiltration (%) per pressure step ΔP (Pa)		
								ΔP0	ΔP150	ΔP450	ΔP0	ΔP150	ΔP450
Olsson [136]	Facade boards	Sealant	Verified working procedure defects	-	No air barrier	EN 12865 B (cyclic)	1.9	0	0	0.002	0.00%	0.00%	0.11%
	Concrete	Sealing strips and sealant						0.001	0.0015	0	0.05%	0.08%	0.00%
	ETICS	Sealant						0.0025	0.006	0.003	0.13%	0.32%	0.16%
	ETICS	Paintable waterproofing						0.022	0.028	0.025	1.16%	1.47%	1.32%
								ΔP0	ΔP75	ΔP600	ΔP0	ΔP75	ΔP600
Olsson [140]	Plaster-based boards	Sealant	Gap at connection with exterior window sill	9 mm^2	No air barrier	EN 12865 A (cyclic)	3.4	0.011	0.027	0.04	0.32%	0.79%	1.18%
				4 mm^2				0.0002	0.003	0.013	0.01%	0.09%	0.38%
								ΔP0	ΔP75	ΔP200	ΔP0	ΔP75	ΔP200

Lacasse et al. [139]	Hardboard siding	J-trim + flashing	Opening in lower corners of window	1 mm diameter	PMMA (0,84)	Static	3.4	0.039	0.059	0.108	1.15%	1.74%	3.18%
		+ rubber gasket						0.032	0.049	0.072	0.94%	1.44%	2.12%
		+ PUR at interior						0.023	0.059	0.069	0.68%	1.74%	2.03%
		+ PUR + drip cap flashing						0.043	0.051	0.063	1.26%	1.50%	1.85%
Lacasse [144]	Hardboard siding	Sealant	Horizontal slit at lower and outer corner	90 mm	PMMA (2,24)	Static		ΔP0	ΔP75	ΔP200	ΔP0	ΔP75	ΔP200
							0.8	0.018	0.015	0.019	2.25%	1.88%	2.38%
							1.6	0.095	0.13	0.13	5.94%	8.13%	8.13%
							3.4	0.165	0.165	0.17	4.85%	4.85%	5.00%
Lacasse et al. [137]		Sealant	Missing sealant length at horizontal and vertical joint	90 mm	PMMA (0,72)	Static		ΔP0		ΔP300	ΔP0		ΔP300
	Stucco						1.7	0.0069	-	0.087	0.41%	-	5.12%
	EIFS							0.058	-	0.088	3.41%	-	5.18%
	Hardboard siding							0.003	-	0.013	0.18%	-	0.76%
								ΔP0		ΔP300	ΔP0		ΔP300
	Stucco						3.4	0	-	0.074	0.00%	-	2.18%
	EIFS							0.108	-	0.2	3.18%	-	5.88%
	Hardboard siding							0	-	0.004	0.00%	-	0.12%
Sahal and Lacasse [138]	Hardboard lap siding	Sealant	Missing sealant length at lower and outer corner	90 mm		Static (Spraying water)		ΔP0	ΔP75	ΔP600	ΔP0	ΔP75	ΔP600
					PMMA (0,84)		3.4	0.23	0.20	0.49	6.76%	5.88%	14.41%
					PMMA (1,12)			0.20	0.25	0.55	5.88%	7.35%	16.18%
					PMMA (1,68)			0.23	0.27	0.61	6.76%	7.94%	17.94%
					PMMA (1,68)	Static (Cascade water)		ΔP0	ΔP75	ΔP600	ΔP0	ΔP75	ΔP600
							1	0.28	0.29	0.69	28.00%	29.00%	69.00%
							3	0.22	0.29	0.86	7.33%	9.67%	28.67%
							5	0.42	0.58	1.50	8.40%	11.60%	30.00%
Ngudjiharto [90]	Vinyl siding	J-trim	No	-	Polyethylene sheet	Field	0-2	-	-	-	-	-	0.55%
	Stucco	Sealant	Missing sealant at corner	100 mm			0-2,5	-	-	-	-	-	1.50%

Table A 9: Water infiltration rates and percentages through the interface between walls and circular ducts

Ref.	Exterior surface	Sealing method	Deficiency type	Dimensions	Air barrier ($m^3/h.m^2$ @ 50 Pa)	Test procedure	Spray rate ($L/min.m^2$)	Infiltration (L/min) per pressure step ΔP (Pa)			Infiltration (%) per pressure step ΔP (Pa)		
								ΔP0	ΔP75	ΔP300	ΔP0	ΔP75	ΔP300
Olsson [140]	Plaster-based boards	Sealant	Visible opening above duct	35 x 0,9 mm	No air barrier	EN 12865 Procedure A	3.4	0.036	0.036	0.036	1.06%	1.06%	1.06%
Lacasse et al. [137]	Acrylic sheathed wall	Sealant	Missing sealant length above duct	1 x 90 mm	PMMA (ELA of 120 mm2			ΔP0	ΔP75	ΔP300	ΔP0	ΔP75	ΔP300
						Static	3.9	0.14	0.17	0.27	3.59%	4.36%	6.92%
						Static	6.07	0.44	0.56	0.63	7.25%	9.23%	10.38%
						Dynamic	3.9	-	0.14	0.2	-	3.59%	5.13%
						Dynamic	6.07	-	0.46	0.55	-	7.58%	9.06%
		Sealant	Missing sealant length above duct	1 x 50 mm	PMMA (0,56)	Static	1.7	ΔP0		ΔP300	ΔP0		ΔP300
	Stucco							0.191	-	0.113	11.24%	-	6.65%
	EIFS							0.083	-	0.14	4.88%	-	8.24%
	Masonry							0	-	0.018	0.00%	-	1.06%
	Hardboard siding							0.008	-	0.019	0.47%	-	1.12%

								ΔP0		ΔP300	ΔP0		ΔP300
	Stucco							0.254	-	0.34	7.47%	-	10.00%
	EIFS						3.4	0.066	-	0.218	1.94%	-	6.41%
	Masonry							0.028	-	0.12	0.82%	-	3.53%
	Hardboard siding							0.042	-	0.042	1.24%	-	1.24%
								ΔP0	ΔP75	ΔP300	ΔP0	ΔP75	ΔP300
							0.58	0.00031	0.00117	0.00424	0.05%	0.20%	0.73%
Saber [119]	Fibre-cement	Sealant	Openings in sealant above duct	2,5 mm diameter	Acryclic sheathing		1.16	0.00036	0.00084	0.00611	0.03%	0.07%	0.53%
							1.74	0.00056	0.00128	0.00729	0.03%	0.07%	0.42%
								ΔP0	ΔP75	ΔP600	ΔP0	ΔP75	ΔP600
					PMMA (0,84)			0.11	0.11	0.11	3.24%	3.24%	3.24%
					PMMA (1,12)	Static (Spraying water)	3.4	0.14	0.14	0.12	4.12%	4.12%	3.53%
Sahal and Lacasse [138]	Hardboard lap siding	Sealant	Missing sealant above duct	50 mm	PMMA (1,68)			0.08	0.08	0.13	2.35%	2.35%	3.82%
								ΔP0	ΔP75	ΔP600	ΔP0	ΔP75	ΔP600
							1	0.14	0.12	0.11	14.00%	12.00%	11.00%
					PMMA (1,68)	Static (Cascade water)	3	0.10	0.20	0.37	3.33%	6.67%	12.33%
							5	0.21	0.22	0.50	4.20%	4.40%	10.00%

Table A 10: Water infiltration rates and percentages through the interface between walls and rectangular ducts

Ref.	Exterior surface	Sealing method	Deficiency type	Dimensions	Air barrier ($m^3/h.m^2$ @ 50 Pa)	Test procedure	Spray rate ($L/min.m^2$)	Infiltration (L/min) per pressure step ΔP (Pa)			Infiltration (%) per pressure step ΔP (Pa)		
								ΔP0	ΔP75	ΔP300	ΔP0	ΔP75	ΔP300
Olsson [140]	Plaster-based boards	Sealant	Visible openings above duct	30 x 2 mm	No air barrier	EN 12865 A (cyclic)	3.4	0.001	0.005	0.06	0.03%	0.15%	1.76%
								ΔP0	ΔP75	ΔP300	ΔP0	ΔP75	ΔP300
						Static	3.9	0.06	0.08	0.14	1.54%	2.05%	3.59%
	Acrylic sheathed wall	Sealant	Missing sealant length above duct	1 x 45 mm	PMMA (ELA of 120 mm2	Static	6.07	0.06	0.24	0.3	0.99%	3.95%	4.94%
						Dynamic	3.9	-	0.08	0.17	-	2.05%	4.36%
						Dynamic	6.07	-	0.15	0.28	-	2.47%	4.61%
								ΔP0		ΔP300	ΔP0		ΔP300
	Stucco							0.0765	-	0.069	4.50%	-	4.06%
Lacasse et al. [137]	EIFS						1.7	0.204	-	0.233	12.00%	-	13.71%
	Masonry							0.145	-	-	8.53%	-	-
	Hardboard siding							0.092	-	0.099	5.41%	-	5.82%
		Sealant	Missing sealant length above duct	1 x 50 mm	PMMA (0,56)	Static		ΔP0		ΔP300	ΔP0		ΔP300
	Stucco							0.047	-	0.2	1.38%	-	5.88%
	EIFS						3.4	0.256	-	0.249	7.53%	-	7.32%
	Masonry							0.115	-	-	3.38%	-	-
	Hardboard siding							0.167	-	0.154	4.91%	-	4.53%
								ΔP0	ΔP75	ΔP600	ΔP0	ΔP75	ΔP600
Sahal and Lacasse [138]	Hardboard lap siding	Sealant	Missing sealant above duct	50 mm	PMMA (0,84)	Static (Spraying water)	3.4	0.05	0.05	0.05	1.47%	1.47%	1.47%
					PMMA (1,12)			0.06	0.07	0.06	1.76%	2.06%	1.76%

PMMA (1,68)			0.08	0.07	0.05	2.35%	2.06%	1.47%
			ΔP0	ΔP75	ΔP600	ΔP0	ΔP75	ΔP600
PMMA (1,68)	Static (Cascade water)	1	0.06	0.05	0.07	6.00%	5.00%	7.00%
		3	0.12	0.12	0.12	4.00%	4.00%	4.00%
		5	0.19	0.20	0.21	3.80%	4.00%	4.20%

Table A 11: Water infiltration rates and percentages through linear joints

Ref.	Exterior surface	Sealing method	Deficiency type	Dimensions	Air barrier ($m^3/h.m^2$ @ 50 Pa)	Test procedure	Spray rate ($L/min.m^2$)	Infiltration (L/min) per pressure step ΔP (Pa)			Infiltration (%) per pressure step ΔP (Pa)		
								ΔP0	ΔP75	ΔP500	ΔP0	ΔP75	ΔP500
Lacasse et al. [143]	PMMA	Sealant	Crack at side of vertical joint	2 mm	No air barrier	Static	4.00	0.000	0.000	0.004	0.00%	0.00%	0.09%
				4 mm				0.000	0.000	0.003	0.00%	0.00%	0.09%
				16 mm				0.000	0.000	0.002	0.00%	0.00%	0.04%
				2 x 2 mm				0.000	0.003	0.006	0.00%	0.08%	0.14%
				2 x 8 mm				0.004	0.006	0.010	0.10%	0.14%	0.24%
				2 x 16 mm				0.010	0.010	0.012	0.25%	0.25%	0.30%
								ΔP0	ΔP75	ΔP500	ΔP0	ΔP75	ΔP500
			Crack at bottom of horizontal joint	4 mm				0.000	0.000	0.000	0.00%	0.00%	0.00%
				16 mm				0.000	0.000	0.000	0.00%	0.00%	0.01%
				2 x 8 mm				0.000	0.019	0.105	0.00%	0.48%	2.63%
				2 x 16 mm				0.000	0.014	0.139	0.00%	0.35%	3.48%

References

[1] V. P. de Freitas, “A state-of-the-art report on building pathology,” CIB-W086 Building Pathology, 2013.

[2] “Observatoire de la qualité de la construction Edition 2021.” Agence Qualité Construction, 2021.

[3] M. J. Carretero-Ayuso, A. Moreno-Cansado, and J. de Brito, “General Survey of Construction-Related Complaints in Recent Buildings in Spain,” *Int J Civ Eng*, vol. 16, no. 12, pp. 1781–1796, 2018, doi: 10.1007/s40999-017-0259-7.

[4] J. De Vos, A. Blommaert, and N. Van Den Bossche, “Statistical Analysis on Belgian Building Defects,” Barcelona, Spain, 2020. doi: 10.23967/dbmc.2020.130.

[5] D. Zirkelbach, Th. Schmidt, M. Kehrer, and H. M. Künzel, “WUFI-Pro-5_Manual.”

[6] H. Künzel, “Simultaneous Heat and Moisture Transport in Building Components: One-and two-dimensional calculation,” Fraunhofer Institute of Building Physics, 1995.

[7] J. Grunewald, “Diffusiver und konvektiver Stoff- und Energietransport in kapillarporösen Baustoffen,” Doctoral Thesis, Technischen Universität Dresden, Dresden, 1997.

[8] H. M. Künzel, “Accounting for unintended moisture sources in hygrothermal building analysis,” in *NSB 2014 Building Physics Conference*, 2014, p. 7.

[9] H. M. Künzel, D. Zirkelbach, A. Karagiozis, A. Holm, and K. Sedlbauer, “Simulating Water Leaks in External Walls to Check the Moisture Tolerance of Building Assemblies in Different Climates,” in *11DBMC International Conference on Durability of Building Materials and Components*, Istanbul, Turkey, 2008, p. 8.

[10] H. Ge and R. Krpan, “Wind-driven Rain Study in the Coastal Climate of British Columbia,” British Columbia Institute of Technology, British Columbia, 2009.

[11] H. Ge, U. K. Deb Nath, and V. Chiu, “Field measurements of wind-driven rain on mid-and high-rise buildings in three Canadian regions,” *Building and Environment*, vol. 116, pp. 228–245, May 2017, doi: 10.1016/j.buildenv.2017.02.016.

[12] S. M. Cornick, M. A. Lacasse, B. Hardman, C. G. Carll, T. Weston, and S. W. Dean, “An Investigation of Climate Loads on Building Façades for Selected Locations in the United States,” *J. ASTM Int.*, vol. 6, no. 2, p. JAI101210, 2009, doi: 10.1520/JAI101210.

[13] S. Kim, D. Zirkelbach, and H. M. Künzel, “Wind-driven rain exposure on building envelopes taking into account frequency distribution and correlation with different wall orientations,” *Building and Environment*, p. 108665, Dec. 2021, doi: 10.1016/j.buildenv.2021.108665.

[14] B. Blocken and J. Carmeliet, “A review of wind-driven rain research in building science,” *Journal of Wind Engineering and Industrial Aerodynamics*, vol. 92, no. 13, pp. 1079–1130, Nov. 2004, doi: 10.1016/j.jweia.2004.06.003.

[15] A. Kubilay, D. Derome, B. Blocken, and J. Carmeliet, “High-resolution field measurements of wind-driven rain on an array of low-rise cubic buildings,” *Building and Environment*, vol. 78, pp. 1–13, Aug. 2014, doi: 10.1016/j.buildenv.2014.04.004.

[16] T. Baheru, A. G. Chowdhury, J.-P. Pinelli, and G. Bitsuamlak, “Distribution of wind-driven rain deposition on low-rise buildings: Direct impinging raindrops versus surface runoff,” *Journal of Wind Engineering and Industrial Aerodynamics*, vol. 133, pp. 27–38, Oct. 2014, doi: 10.1016/j.jweia.2014.06.023.

[17] E. C. C. Choi, “Criteria for water penetration testing,” ASTM STP 1314, 1998.

[18] V. Etyemezian, “Impingement of rain drops on a tall building,” *Atmospheric Environment*, vol. 34, no. 15, pp. 2399–2412, 2000, doi: 10.1016/S1352-2310(99)00443-4.

[19] J. Straube and E. F. P. Burnett, “Simplified prediction of driving rain on buildings, international building physics conference,” in *International Building Physics Conference*, Eindhoven, the Netherlands, 2000, pp. 375–382.

[20] E. Cho, C. Yoo, M. Kang, S. Song, and S. Kim, “Experiment of wind-driven-rain measurement on building walls and its in-situ validation,” *Building and Environment*, vol. 185, p. 107269, Nov. 2020, doi: 10.1016/j.buildenv.2020.107269.

[21] M. Abuku, H. Janssen, J. Poesen, and S. Roels, “Impact, absorption and evaporation of raindrops on building facades,” *Building and Environment*, vol. 44, no. 1, pp. 113–124, Jan. 2009, doi: 10.1016/j.buildenv.2008.02.001.

[22] R. Couper, “Factors affecting the production of surface runoff from wind-driven rain,” presented at the RILEM Symposium on Moisture Problems in Buildings, 1974.

[23] A. Erkal, D. D’Ayala, and L. Sequeira, “Assessment of wind-driven rain impact, related surface erosion and surface strength reduction of historic building materials,” *Building and Environment*, vol. 57, pp. 336–348, 2012, doi: 10.1016/j.buildenv.2012.05.004.

[24] A. L. Yarin, “DROP IMPACT DYNAMICS: Splashing, Spreading, Receding, Bouncing…,” *Annual Review of Fluid Mechanics*, vol. 38, no. 1, pp. 159–192, 2006, doi: 10.1146/annurev.fluid.38.050304.092144.

[25] S. Chandra and C. Avedisian, “Observations of droplet impingement on a ceramic porous surface,” *International Journal of Heat and Mass Transfer*, vol. 35, no. 10, 1992, doi: 10.1016/0017-9310(92)90080-C.

[26] M. Rein, “Phenomena of liquid drop impact on solid and liquid surfaces,” *Fluid Dyn. Res.*, vol. 12, no. 2, pp. 61–93, Aug. 1993, doi: 10.1016/0169-5983(93)90106-K.

[27] M.-J. Wang, F.-H. Lin, Y.-L. Hung, and S.-Y. Lin, “Dynamic Behaviors of Droplet Impact and Spreading: Water on Five Different Substrates,” *Langmuir*, vol. 25, no. 12, pp. 6772–6780, Jun. 2009, doi: 10.1021/la9002862.

[28] B. J. Mason and J. B. Andrews, “Drop-size distributions from various types of rain,” *Q.J Royal Met. Soc.*, vol. 86, no. 369, pp. 346–353, Jul. 1960, doi: 10.1002/qj.49708636906.

[29] C. K. Mutchler and L. M. Hansen, “Splash of a waterdrop at terminal velocity,” *Science*, vol. 169, no. 3952, pp. 1311–1312, Sep. 1970, doi: 10.1126/science.169.3952.1311.

[30] O. Beijer, “Concrete walls and weathering,” presented at the RILEM/ASTM/CIB Symposium on evaluation of the performance of external vertical surfaces of buildings, 1977.

[31] M. El-Shimi, R. White, and P. Fazio, “Influence of facade geometry on weathering,” *Canadian Journal of Civil Engineering*, vol. 7, no. 4, pp. 597–613, 1980.

[32] C. Hall and A. N. Kalimeris, “Water movement in porous building materials—V. Absorption and shedding of rain by building surfaces,” *Building and Environment*, vol. 17, no. 4, pp. 257–262, Jan. 1982, doi: 10.1016/0360-1323(82)90018-X.

[33] C. Hall and M. H. Raymond Yau, “Water movement in porous building materials—IX. The water absorption and sorptivity of concretes,” *Building and Environment*, vol. 22, no. 1, pp. 77–82, Jan. 1987, doi: 10.1016/0360-1323(87)90044-8.

[34] C. Hall, “Water movement in porous building materials—I. Unsaturated flow theory and its applications,” *Building and Environment*, vol. 12, no. 2, pp. 117–125, Jan. 1977, doi: 10.1016/0360-1323(77)90040-3.

[35] R. J. Gummerson, C. Hall, and W. D. Hoff, “Water Movement in Porous Building Materia.ls--II. Hydraulic Suction and Sorptlvlty of Brick and Other Masonry Materials,” *Building and Environment*, vol. 15, p. 8.

[36] C. Hall, “Water movement in porous building materials—IV. The initial surface absorption and the sorptivity,” *Building and Environment*, vol. 16, no. 3, pp. 201–207, Jan. 1981, doi: 10.1016/0360-1323(81)90014-7.

[37] C. Hall, W. D. Hoff, and M. R. Nixon, “Water movement in porous building materials—VI. Evaporation and drying in brick and block materials,” *Building and Environment*, vol. 19, no. 1, pp. 13–20, Jan. 1984, doi: 10.1016/0360-1323(84)90009-X.

[38] C. Hall and T. K.-M. Tse, “Water movement in porous building materials—VII. The sorptivity of mortars,” *Building and Environment*, vol. 21, no. 2, pp. 113–118, Jan. 1986, doi: 10.1016/0360-1323(86)90017-X.

[39] B. Blocken, D. Derome, and J. Carmeliet, “Rainwater runoff from building facades: A review,” *Building and Environment*, vol. 60, pp. 339–361, Feb. 2013, doi: 10.1016/j.buildenv.2012.10.008.

[40] Á. Mas, J. Gutiérrez, E. Gil, A. Gil, and V. Galvañ, “Design and construction recommendations to improve impermeability in rainscreen walls built with natural stone coverings,” *Construction and Building Materials*, vol. 25, no. 4, pp. 1753–1761, Apr. 2011, doi: 10.1016/j.conbuildmat.2010.11.091.

[41] N. Van Den Bossche, M. Lacasse, T. Moore, and A. Janssens, “Water infiltration through openings in a vertical plane under static boundary conditions,” presented at the Proceedings of the 5th International Building Physics Conference, Kyoto, Japan, 2012.

[42] K. Calle and N. Van Den Bossche, “Phenomenologic analysis on the moisture flux through cracks in masonry constructions,” in *International RILEM Conference on Materials, Systems and Structures in Civil Engineering*, Lyngby, Denmark, 2016, p. 11.

[43] L. Olsson and C.-E. Hagentoft, “New algorithm for water leakages flow through rain screen deficiencies,” in *Healthy, Intelligent and Resilient Buildings and Urban Environments*, 2018, pp. 1055–1060. doi: 10.14305/ibpc.2018.ms-3.03.

[44] L. Olsson, “Rain intrusion rates at façade details – a summary of results from four laboratory studies,” *Energy Procedia*, vol. 132, pp. 387–392, Oct. 2017, doi: 10.1016/j.egypro.2017.09.639.

[45] T. V. Moore and M. A. Lacasse, “Approach to Incorporating Water Entry and Water Loads to Wall Assemblies When Completing Hygrothermal Modelling,” in *Building Science and the Physics of Building Enclosure Performance*, D. J. Lemieux and J. Keegan, Eds. 100 Barr Harbor Drive, PO Box C700, West Conshohocken, PA 19428-2959: ASTM International, 2020, pp. 157–176. doi: 10.1520/STP161720180088.

[46] G. D. Meersman, N. Van Den Bossche, and A. Janssens, “HAM simulation of the drying out capacity of water ingress in wooden constructions,” in *Nordic Symposium on Building Physics*, 2014, p. 8.

[47] P. Beaulieu *et al.*, “Final Report from Task 8 of MEWS Project (T8-03) - Hygrothermal Response of Exterior Wall Systems to Climate Loading: Methodology and Interpretation of Results for Stucco, EIFS, Masonry and Siding Clad Wood-Frame Walls,” National Research Council of Canada, Canada, 2002.

[48] K. Calle, C. Coupillie, A. Janssens, and N. Van Den Bossche, “Implementation of rainwater infiltration measurements in hygrothermal modelling of non-insulated brick cavity walls,” *Journal of Building Physics*, vol. 43, no. 6, pp. 477–502, May 2020, doi: 10.1177/1744259119883909.

[49] A. Teasdale-St-Hilaire and D. Derome, “State-of-the-Art Review of Simulated Rain Infiltration and Environmental Loading for Large-Scale Building Envelope Testing,” *ASHRAE Transactions*, vol. 111, pp. 389–401, 2005.

[50] M. Kumaran *et al.*, “An Integrated methodology to develop moisture management strategies for exterior wall systems.” National Research Council Canada, Jan. 01, 2003.

[51] N. Van Den Bossche, S. Van Goethem, S. Scharlaken, S. Sulmon, and A. Janssens, “Watertightness and water management of curtain walls,” in *Proceedings of the 1st International Symposium on Building Pathology*, 2015, p. 8.

[52] I. Samuelson, K. Mjörnell, and A. Jansson, “Moisture damage in rendered, undrained, well insulated stud walls,” *8th Nordic Symposium on Building Physics*, p. 8, 2008.

[53] T. Kvande, N. Bakken, E. Bergheim, and J. Thue, “Durability of ETICS with Rendering in Norway—Experimental and Field Investigations,” *Buildings*, vol. 8, no. 7, p. 93, Jul. 2018, doi: 10.3390/buildings8070093.

[54] J. C. Z. Piaia, M. Cheriaf, J. C. Rocha, and N. L. Mustelier, “Measurements of water penetration and leakage in masonry wall: Experimental results and numerical simulation,” *Building and Environment*, vol. 61, pp. 18–26, 2013, doi: 10.1016/j.buildenv.2012.11.017.

[55] NAHB Research Center, “Water intrusion evaluation for caulkless siding, window and door systems,” U.S. Department of Housing and Urban Development, Washington DC, 2002.

[56] J. Lstiburek, “Rainwater Management Performance of Newly Constructed Residential Building Enclosures During August and September 2004.” Building Science Press, 2006.

[57] R. Minkovich, “Installing water-managed synthetic stucco.” Journal of light construction, 1998.

[58] J. Lstiburek, “BSI-102: The Coming Stucco-Pocalypse.” Building Science Corporation, 2018.

[59] M. T. Williams and J. Kistler, “Utilizing a Modified AAMA 501.1 Dynamic Wind Generation to Simulate Wind-Driven Rain in Windows, Curtain Walls, Architectural Metal Walls, Masonry, EIFS, and Concrete Facades,” in *Building Walls Subject to Water Intrusion and Accumulation: Lessons from the Past and Recommendations for the Future*, West Conshohocken, 2014, vol. 1549, pp. 92–112. doi: 10.1520/STP154920130042.

[60] S. G. Naggatz and S. F. Sinusas, “Water Leakage Testing of Glass and Metal Curtain Walls,” in *Building Walls Subject to Water Intrusion and Accumulation: Lessons from the Past and Recommendations for the Future*, West Conshohocken, 2014, vol. 1549, pp. 143–165. doi: 10.1520/STP154920130046.

[61] A. Teasdale-St-Hilaire, D. Derome, and P. Fazio, “Development of an experimental methodology for the simulation of wetting due to rain infiltration for building envelope testing,” in *Research in Building Physics*, Leiden, 2003, pp. 455–462.

[62] F. Raji, I. Zisis, and J. P. Pinelli, “Experimental Investigation of Wind-Driven Rain Propagation in a Building Interior,” *Journal of Structural Engineering*, vol. 146, no. 7, p. 04020114, Jul. 2020, doi: 10.1061/(ASCE)ST.1943-541X.0002670.

[63] M. Kahangi, “Resistance of Clay Brick Masonry Façades to Wind-Driven Rain - Repointing of Eroded Mortar Joints,” Licentiate Thesis, Lund University, 2021.

[64] E. A. Laycock and C. Wood, “Understanding and controlling the ingress of driven rain through exposed, solid wall masonry structures,” *Geological Society, London, Special Publications*, vol. 391, no. 1, pp. 175–191, Jan. 2014, doi: 10.1144/SP391.1.

[65] L. Olsson, “Rain resistance of façades with façade details: A summary of three field and laboratory studies,” *Journal of Building Physics*, vol. 41, no. 6, pp. 521–532, May 2018, doi: 10.1177/1744259117713265.

[66] R. A. Van Straaten, G. A. Kopp, and J. F. Straube, “Testing Water Penetration Resistance of Window Systems to Realistic Dynamic Air Pressures,” presented at the Proceedings of the International Conference of Building Enclosure Science & Technology, 2010.

[67] C. T. Salzano, F. J. Masters, and J. D. Katsaros, “Water penetration resistance of residential window installation options for hurricane-prone areas,” *Building and Environment*, vol. 45, no. 6, pp. 1373–1388, Jun. 2010, doi: 10.1016/j.buildenv.2009.12.002.

[68] RDH Building Engineering, “Water penetration resistance of windows,” Canada Mortgage and Housing Corporation, Vancouver, 2002.

[69] L. Olsson, “Results from laboratory tests of wind driven rain tightness in more than 100 facades and weather barriers,” in *NSB 2014 Building Physics Conference*, 2014, p. 7.

[70] C. Lopez, F. J. Masters, and S. Bolton, “Water penetration resistance of residential window and wall systems subjected to steady and unsteady wind loading,” *Building and Environment*, vol. 46, no. 7, pp. 1329–1342, Jul. 2011, doi: 10.1016/j.buildenv.2010.12.008.

[71] N. Van Den Bossche and A. Janssens, “Airtightness and watertightness of window frames: Comparison of performance and requirements,” *Building and Environment*, vol. 110, pp. 129–139, Dec. 2016, doi: 10.1016/j.buildenv.2016.09.034.

[72] P. E. Beers and W. D. Smith, “Evaluation of field water infiltration test results of windows and sliding glass door assemblies installed in new construction projects,” *ASTM STP 1352 Water problems in building exterior walls: Evaluation, prevention and repair*, 1999.

[73] F. Rädel and J. Lange, “Dichtigkeit von Sandwichelementkonstruktionen - Wasser- und Luftdichtigkeit in Längs- und Fensteranschlussfugen,” *Stahlbau*, vol. 87, no. 7, pp. 687–694, 2018, doi: 10.1002/stab.201810626.

[74] E. S. Farrington, T. Anderson, L. Grant, and R. Seraderian, “Precast concrete–to–precast concrete facade joints using precompressed expandable foam,” *PCI Journal*, p. 12, 2019.

[75] W. Van As, “Investigation into the possibilities of improving raintightness of wooden windows, doors and frames in brickwork,” presented at the Symposium on weathertight joints for walls, 1969.

[76] M. R. Bassett, J. C. Burgess, and M. J. Camilleri, “The weathertightness of window-to-wall joints - dependency on installation details,” in *IRHACE Annual Conference*, Hamilton, 2003, p. 11.

[77] S. Van Linden and N. Van Den Bossche, “Watertightness performance of face-sealed versus drained window-wall interfaces,” *Building and Environment*, vol. 196, p. 107824, Jun. 2021, doi: 10.1016/j.buildenv.2021.107824.

[78] “ASHRAE 160-Criteria for Moisture-Control Design Analysis in Buildings.” ASHRAE, 2016.

[79] H. Saber, M. Lacasse, and T. Moore, “Hygrothermal Performance Assessment of Stucco-Clad Wood Frame Walls Having Vented and Ventilated Drainage Cavities,” 2017, pp. 198–231. doi: 10.1520/STP159920160100.

[80] L. Wang and H. Ge, “Effect of rain leakage on hygrothermal performance of highly insulated wood-framed walls: a stochastic approach,” *Can. J. Civ. Eng.*, vol. 46, no. 11, pp. 979–989, 2019, doi: 10.1139/cjce-2019-0223.

[81] K. Carbonez, H. Ge, and A. Janssens, “Comparison between uniform rain loads and point sources to simulate rainwater leakage with commercial HAM-models,” in *1st International Symposium on Building Pathology*, Porto, Portugal, 2015, p. 8.

[82] N. Sahal and M. A. Lacasse, “Proposed method for calculating water penetration test parameters of wall assemblies as applied to Istanbul, Turkey,” *Building and Environment*, vol. 43, no. 7, pp. 1250–1260, Jul. 2008, doi: 10.1016/j.buildenv.2007.03.009.

[83] M. A. Recatalá, S. G. Morales, and N. Van den Bossche, "Pressure-equalised façade systems: Evaluation of current watertightness test standards used to assess the performance of enclosure components," *Journal of Building Physics*, vol. 43, no. 5, pp. 369–397, Mar. 2020, doi: 10.1177/1744259119880284.

[84] N. Van Den Bossche, "Watertightness of building components - Principles, testing and design guidelines," Doctoral Thesis, Ghent university, Ghent, Belgium, 2013.

[85] "EN 1027 Windows and doors - Water tightness - Test method." European Committee for Standardization, 2016.

[86] "EN 12865 Hygrothermal performance of building components and building elements - Determination of the resistance of external wall systems to driving rain under pulsating air pressure." European Committee for Standardization, 2001.

[87] M. Y. L. Chew, "A modified on-site water chamber tester for masonry walls," *Construction and Building Materials*, vol. 15, no. 7, pp. 329–337, Oct. 2001, doi: 10.1016/S0950-0618(01)00011-3.

[88] J. M. Pérez-Bella, J. Domínguez-Hernández, E. Cano-Suñén, J. J. del Coz-Díaz, and F. J. Suárez-Domínguez, "A comparison of methods for determining watertightness test parameters of building façades," *Building and Environment*, vol. 78, pp. 145–154, Aug. 2014, doi: 10.1016/j.buildenv.2014.04.027.

[89] N. Van Den Bossche, M. A. Lacasse, and A. Janssens, "A uniform methodology to establish test parameters for watertightness testing - Part I: A critical review," *Building and Environment*, vol. 63, pp. 145–156, May 2013, doi: 10.1016/j.buildenv.2012.12.003.

[90] E. Ngudjiharto, "Field Study of Wind Driven Rain Penetration into Vinyl Sidings and Stucco-Clad Wood-Frame Wall Systems at Window Sill," Master Thesis, Concordia University, Montreal, Quebec, Canada, 2015.

[91] S. Cornick and M. Lacasse, "A Review of Climate Loads Relevant to Assessing the Watertightness Performance of Walls, Windows, and Wall-Window Interfaces," *J. ASTM Int.*, vol. 2, no. 10, p. 12505, 2005, doi: 10.1520/JAI12505.

[92] J. M. Pérez-Bella, J. Domínguez-Hernández, B. Rodríguez-Soria, J. J. del Coz-Díaz, and E. Cano-Suñén, "Combined use of wind-driven rain and wind pressure to define water penetration risk into building façades: The Spanish case," *Building and Environment*, vol. 64, pp. 46–56, Jun. 2013, doi: 10.1016/j.buildenv.2013.03.004.

[93] N. Van Den Bossche, M. A. Lacasse, and A. Janssens, "A uniform methodology to establish test parameters for watertightness testing part II: Pareto front analysis on co-occurring rain and wind," *Building and Environment*, vol. 63, pp. 157–167, May 2013, doi: 10.1016/j.buildenv.2012.12.019.

[94] Morrison Hershfield, "Survey of building envelope failures in the coastal climate of British Columbia," Canada Mortgage and Housing Corporation, Canada, 1996.

[95] M. E. Waltz and P. E. Nelson, "Wood Siding Weather Protection: Don't Get Caught in the Rain Without It," *J. Thermal Env. & Building Science*, vol. 22, 1999.

[96] H. Yang, Y. Xie, and J. Yuan, "Potential of self-drying siding with raised air cavities for building envelopes," *Building and Environment*, vol. 152, pp. 172–181, Apr. 2019, doi: 10.1016/j.buildenv.2019.02.002.

[97] G. A. Tsongas, D. P. Govan, and J. A. McGillis, "Field Observations and Laboratory Tests of Water Migration in Walls with Shiplap Hardboard Siding," in *Thermal Performance of the Exterior Envelopes of Buildings VII*, Florida, USA, 1998, p. 15.

[98] C. R. Boardman and S. V. Glass, "Investigating Wind-Driven Rain Intrusion in Walls with the CARWASh," *ASHRE 2013, Thermal Performance of the Exterior Envelopes of Whole Buildings XII International Conference*, p. 11, 2013.

[99] "ETAG 004 Guideline for European Technical Approval of External Thermal Insulation Composite Systems (ETICS) with rendering." European Organisation for Technical Approvals, 2013.

[100] W. Brown, J. Ullett, A. Karagiozis, and T. Tonyan, "Barrier EIFS Clad Walls: Results from a Moisture Engineering Study," *Journal of Thermal Insulation and Building Envelopes*, vol. 20, no. 3, pp. 206–226, Jan. 1997, doi: 10.1177/109719639702000304.

[101] T. Remmele, "EIFS Resistance to Water Penetration and Evaluation in Accordance with EIMA Test Method 101.02," in *Exterior Insulation Finish Systems (EIFS): Materials, Properties, and Performance*, P. Nelson and R. Kroll, Eds. West Conshohocken, PA: ASTM International, 1996, pp. 177–185. doi: 10.1520/STP39220S.

[102] E. Barreira and V. P. de Freitas, “Experimental study of the hygrothermal behaviour of External Thermal Insulation Composite Systems (ETICS),” *Building and Environment*, vol. 63, pp. 31–39, May 2013, doi: 10.1016/j.buildenv.2013.02.001.

[103] F. Stazi, C. Di Perna, and P. Munafò, “Durability of 20-year-old external insulation and assessment of various types of retrofitting to meet new energy regulations,” *Energy and Buildings*, vol. 41, no. 7, pp. 721–731, Jul. 2009, doi: 10.1016/j.enbuild.2009.02.008.

[104] H. Hens and J. Carmeliet, “Performance Prediction for Masonry Walls with EIFS Using Calculation Procedures and Laboratory Testing,” *Journal of Thermal Envelope and Building Science*, vol. 25, no. 3, pp. 167–187, Jan. 2002, doi: 10.1177/0075424202025003141.

[105] J. Lstiburek, “RR-0406: Face Sealed vs. Drainable EIFS,” Building Science, 2004.

[106] A. Jansson, “Action against moisture damage in ETIC walls,” in *NSB 2015 Building Physics Conference*, Lund, Sweden, 2014, p. 7.

[107] R. Quirouette and B. Arch, “Review of the NRCC and USG Study of the EIFS Barrier Walls for Wood Framed Houses in Wilmington, North Carolina,” *Journal of Thermal Insulation and Building Envelopes*, vol. 20, no. 4, pp. 350–358, Apr. 1997, doi: 10.1177/109719639702000407.

[108] M. Rousseau, “An Overview of the Survey of Building Envelope Failures in the Coastal Climate of British Columbia, Performed by Morrisson-Hershfield Limited for CMHC (1996),” *Journal of Thermal Envelope and Building Science*, vol. 22, no. 4, pp. 364–367, Apr. 1999, doi: 10.1177/109719639902200411.

[109] M. Horst, “Compatibility and Integration Details: The Keys to Providing Durable EIFS-Clad Exterior Walls,” in *Exterior Insulation and Finish Systems (EIFS): Performance, Progress, and Innovation*, vol. 1585, P. E. Nelson and B. Egan, Eds. West Conshohocken: ASTM International, 2016, pp. 16–51. doi: 10.1520/STP158520150004.

[110] K. Khaled and R. Richman, “Thermal performance impacts of vented EIFS assemblies in the cold climate of Southern Ontario,” *Journal of Building Engineering*, vol. 31, p. 101446, Sep. 2020, doi: 10.1016/j.jobe.2020.101446.

[111] H. M. Künzel and D. Zirkelbach, “Influence of rain water leakage on the hygrothermal performance of exterior insulation systems,” *Building Physics*, p. 8, 2008.

[112] P. E. Nelson and B. Egan, Eds., *Exterior Insulation and Finish Systems (EIFS): Performance, Progress and Innovation*. 100 Barr Harbor Drive, PO Box C700, West Conshohocken, PA 19428-2959: ASTM International, 2016. doi: 10.1520/STP1585-EB.

[113] E. K. Olson and J. A. Taylor, “Retrofitting Barrier Exterior Insulation and Finish System: Methodology and Performance Assessment,” in *Repair, Retrofit, and Inspection of Building Exterior Wall Systems*, vol. 1493, P. G. Johnson and J. M. Boyd, Eds. W Conshohocken: Amer Society Testing and Materials, 2009, pp. 229-+. doi: 10.1520/STP47777S.

[114] J. L. Parracha *et al.*, “Performance parameters of ETICS: Correlating water resistance, bio-susceptibility and surface properties,” *Construction and Building Materials*, vol. 272, p. 121956, Feb. 2021, doi: 10.1016/j.conbuildmat.2020.121956.

[115] J. M. Ullet and W. C. Brown, “Measured Pressure Equalized Performance of an Exterior Insulation Finish System (EIFS) Specimen,” National Research Council Canada, Ottawa, Canada, 1996.

[116] M. Molnar, J. Jönsson, and P.-O. Rosenkvist, “Development of experimental methods to evaluate infiltration of wind- driven rain into external thermal insulation composite systems (ETICS),” *14th International Conference on Durability and Building Materials*, p. 12, 2017.

[117] W. Brown, M. Dietrich, and M. Latimer, “Assessing the Impact of Thickness on the Performance of Stucco Cladding,” in *Buildings IX ASHRAE*, Florida, USA, 2004, p. 13.

[118] F. J. Spagna and S. S. Ruggiero, “Stucco cladding - Lessons learned from problematic facades,” in *Performance of exterior building walls*, West Conshohocken, PA: ASTM, 2003.

[119] H. Saber, M. Lacasse, T. Moore, and M. Nicholls, “Mid-rise wood constructions: investigation of water penetration through cladding and deficiencies,” National Research Council of Canada, Canada, 2014. doi: 10.4224/21274581.

[120] S. Kahangi Shahreza, J. Niklewski, and M. Molnár, “Experimental investigation of water absorption and penetration in clay brick masonry under simulated uniform water spray exposure,” *Journal of Building Engineering*, vol. 43, p. 102583, Nov. 2021, doi: 10.1016/j.jobe.2021.102583.

[121] N. Van Den Bossche, M. Lacasse, and A. Janssens, “Watertightness of Masonry Walls: An Overview,” in *International Conference on Durability of Building Materials and Components*, Porto, 2011, p. 8.
[122] J. Straube and E. F. P. Burnett, “Driving rain and masonry veneer,” *Water leakage through building facades*, vol. ASTM STP 1314, 1998.
[123] H. Hens, S. Roels, and W. Desadeleer, “Rain leakage through veneer walls, built with concrete blocks,” in *CIB W40 meeting*, Glasgow, United Kingdom, 2004, p. 10.
[124] D. Chiovitti, M. Gonçalves, and A. Renzullo, “Performance Evaluation of Water Repellents for Above Grade Masonry,” *Journal of Thermal Envelope and Building Science*, vol. 22, no. 2, pp. 156–168, Oct. 1998, doi: 10.1177/109719639802200208.
[125] A. J. Rathbone, “Rain and air penetration performance of concrete blockwork,” Technical Report 553, 1982.
[126] K. Calle, “Renovatie van historische gevels: redding of doodsteek?,” Doctoral Thesis, Ghent University, Ghent, Belgium, 2020.
[127] R. H. Brown, “Initial effects of clear coatings on water permeance of masonry,” *ASTM International*, p. 16, 1982.
[128] B. Lubelli, R. P. J. van Hees, C. Groot, and J. Gunneweg, “Risks of the Use of Water Repellents on Salt Contaminated Masonry: the Case of a Windmill in the Netherlands / Risiken beim Hydrophobieren von salzhaltigem Mauerweric Fallstudie anhand einer Windmühle in den Niederlanden,” *Restoration of Buildings and Monuments*, vol. 13, no. 5, pp. 319–330, Oct. 2007, doi: 10.1515/rbm-2007-6154.
[129] G. K. Garden, “Rain penetration and control,” National Research Council of Canada, 40, 1963.
[130] M. A. Recatala, S. G. Morales, and N. Van Den Bossche, “Experimental assessment of rainwater management of a ventilated façade,” *Journal of Building Physics*, vol. 42, no. 1, pp. 38–67, Jul. 2018, doi: 10.1177/1744259117719077.
[131] N. Van Den Bossche, A. Janssens, T. Moore, and M. Lacasse, “Development of numerical model for determination of pressure equalization in facades during wet conditions,” *Building and Environment*, vol. 178, p. 106919, Jul. 2020, doi: 10.1016/j.buildenv.2020.106919.
[132] I. R. Killip and D. W. Cheetham, “The prevention of rain penetration through external walls and joints by means of pressure equalization,” *Building and Environment*, vol. 19, no. 2, pp. 81–91, Jan. 1984, doi: 10.1016/0360-1323(84)90033-7.
[133] M. Arce Recatalá and S. G. Morales, “Quantifying Wind-driven Rain Intrusion – A Comparative Study on The Water Management Features of Different Types of Rear-Ventilated Facade Systems,” in *NSB 2020 Building Physics Conference*, 2020, p. 7.
[134] “Properties of rear-ventilated facades,” 2015. https://www.fvhf.de/facade/VHF-System/Merkmale.php (accessed Oct. 29, 2021).
[135] R. Ting, “Evolution of curtain wall design against water infiltration,” presented at the International conference on building envelope systems and technology ICBEST, Bath, 1997.
[136] L. Olsson, “Laboratory study of driving rain resistance of four façade systems with window fittings - Experimental results of leakage flows,” in *Central Europe towards Sustainable Building*, 2016, p. 9.
[137] M. A. Lacasse, T. J. O’Connor, S. Nunes, and P. Beaulieu, “Report from Task 6 of MEWS Project - Experimental Assessment of Water Penetration and Entry into Wood-Frame Wall Specimens - Final Report,” National Research Council of Canada, Canada, 2003.
[138] N. Sahal and M. A. Lacasse, “Water entry function of a hardboard siding-clad wood stud wall,” *Building and Environment*, vol. 40, no. 11, pp. 1479–1491, Nov. 2005, doi: 10.1016/j.buildenv.2004.11.019.
[139] M. A. Lacasse *et al.*, “Assessing the Effectiveness of Wall-Window Interface Details to Manage Rainwater—Selected Results from Window Installation to a Wall Sheathed in Extruded Polystyrene,” *J. ASTM Int.*, vol. 6, no. 9, p. 101270, 2009, doi: 10.1520/JAI101270.
[140] L. Olsson, “Laboratory Study of Rates of Inward Leakage in 7 Gaps in a Façade Exposed to Driving rain or Water splash,” in *Thermal Performance of the Exterior Envelope and Whole Buildings XIII International Conference*, 2016, p. 12.
[141] M. Lacasse and H. Miyauchi, “Water penetration of cladding components - An overview of the vulnerability of sealed joints to water penetration,” presented at the 12th Canadian Conference on Building Science and Technology, Montreal, Quebec, 2009.
[142] R. Woolman, *Resealing of Buildings: A Guide to Good Practice*. Oxford ; Boston: Butterworth-Heinemann Ltd, 1994.

[143] M. A. Lacasse, H. Miyauchi, J. Hiemstra, A. T. Wolf, and S. W. Dean, "Water Penetration of Cladding Components—Results from Laboratory Tests on Simulated Sealed Vertical and Horizontal Joints of Wall Cladding," *J. ASTM Int.*, vol. 6, no. 6, p. 102048, 2009, doi: 10.1520/JAI102048.
[144] M. A. Lacasse *et al.*, "Results on Assessing the Effectiveness of Wall-Window Interface Details to Manage Rainwater," in *11th Canadian Conference on Building Science and Technology*, Banff, Alberta, 2007, p. 15.
[145] M. S. El-Genk and H. H. Saber, "Minimum thickness of a flowing down liquid on a vertical surface," *International Journal of Heat and Mass Transfer*, vol. 44, p. 17, 2001.
[146] T. V. Moore and M. A. Lacasse, "Determining Moisture Source due to Wind Driven Rain for Input to Hygrothermal Simulations Using Experimental Methods," in *Thermal Performance of the Exterior Envelopes of Whole Buildings XIV International Conference*, Florida, 2019, p. 11.
[147] Z. Xiao, E. Dragomirescu, and M. Lacasse, "Assessing Moisture Resilience of Wall Assemblies to Wind-Driven Rain Loads Arising from Climate Change," Doctoral Thesis, University of Ottawa, Ottawa, Canada, 2021.
[148] Z. Xiao, M. A. Lacasse, and E. Dragomirescu, "An analysis of historical wind-driven rain loads for selected Canadian cities," *Journal of Wind Engineering and Industrial Aerodynamics*, vol. 213, p. 104611, Jun. 2021, doi: 10.1016/j.jweia.2021.104611.
[149] M. J. Fernández, "Study of influence of wind pressure and rain conditions in rain screen walls," *Structural Survey*, vol. 28, no. 1, pp. 46–52, Jan. 2010, doi: 10.1108/02630801011040851.